Allosteric Gating of a Large Conductance Ca-activated K^+ Channel

D.H. Cox, J. Cui, and R.W. Aldrich

From the Department of Molecular and Cellular Physiology, and Howard Hughes Medical Institute, Stanford University, Stanford, California 94305

ABSTRACT Large-conductance Ca-activated potassium channels (BK channels) are uniquely sensitive to both membrane potential and intracellular Ca^{2+}. Recent work has demonstrated that in the gating of these channels there are voltage-sensitive steps that are separate from Ca^{2+} binding steps. Based on this result and the macroscopic steady state and kinetic properties of the cloned BK channel *mslo*, we have recently proposed a general kinetic scheme to describe the interaction between voltage and Ca^{2+} in the gating of the *mslo* channel (Cui, J., D.H. Cox, and R.W. Aldrich. 1997. *J. Gen. Physiol.* In press.). This scheme supposes that the channel exists in two main conformations, closed and open. The conformational change between closed and open is voltage dependent. Ca^{2+} binds to both the closed and open conformations, but on average binds more tightly to the open conformation and thereby promotes channel opening. Here we describe the basic properties of models of this form and test their ability to mimic *mslo* macroscopic steady state and kinetic behavior. The simplest form of this scheme corresponds to a voltage-dependent version of the Monod-Wyman-Changeux (MWC) model of allosteric proteins. The success of voltage-dependent MWC models in describing many aspects of *mslo* gating suggests that these channels may share a common molecular mechanism with other allosteric proteins whose behaviors have been modeled using the MWC formalism. We also demonstrate how this scheme can arise as a simplification of a more complex scheme that is based on the premise that the channel is a homotetramer with a single Ca^{2+} binding site and a single voltage sensor in each subunit. Aspects of the *mslo* data not well fitted by the simplified scheme will likely be better accounted for by this more general scheme. The kinetic schemes discussed in this paper may be useful in interpreting the effects of BK channel modifications or mutations.

KEY WORDS: potassium channel • BK channel • Monod-Wyman-Changeux model • relaxation kinetics • *mslo*

INTRODUCTION

Large conductance Ca-activated potassium channels (BK channels) sense changes in both intracellular Ca^{2+} concentration and membrane voltage. They therefore can act as a point of communication between cellular processes that involve these two common means of signaling. Although progress has been made in understanding the Ca-dependent properties of BK channel gating (McManus and Magleby, 1991; for review see McManus, 1991), the relationship between the mechanism by which Ca^{2+} activates the channel, and that by which voltage activates the channel is less clear. To understand this relationship further, we have recently examined the macroscopic steady state and kinetic properties of the BK channel clone *mslo* over a wide range of Ca^{2+} concentrations and membrane voltages (Cox et al., 1997; Cui et al., 1997). From these studies, and work from other laboratories, several conclusions can be drawn. (*a*) There are charges intrinsic to the channel protein that sense changes in the transmembrane electric field, and thereby confer voltage dependence on *mslo* gating (Methfessel and Boheim, 1982; Blair and Dionne, 1985; Pallotta, 1985; Singer and Walsh, 1987; Wei et al., 1994; Meera et al., 1996; Cui et al., 1997). (*b*) The *mslo* channel can be nearly maximally activated without binding Ca^{2+} (Cui et al., 1997). (*c*) At most Ca^{2+} concentrations and membrane voltages, Ca^{2+} binding steps equilibrate rapidly relative to those that limit the channel's kinetic behavior (Methfessel and Boheim, 1982; Moczydlowski and Latorre, 1983; Cui et al., 1997). (*d*) At least 3 Ca^{2+} binding sites are involved in activation by Ca^{2+} (Barrett et al., 1982; McManus et al., 1985; Golowasch et al., 1986; Cornejo et al., 1987; Oberhauser et al., 1988; Carl and Sanders, 1989; Reinhart et al., 1989; Mayer et al., 1990; McManus and Magleby, 1991; Markwardt and Isenberg, 1992; Perez et al., 1994; Art et al., 1995; Cui et al., 1997). (*e*) Gating steps that do not involve Ca^{2+} binding are highly cooperative (Cui et al., 1997).

To test these conclusions, as well as to gain new insights into BK channel gating, we have attempted to develop a physically reasonable kinetic model that is consistent with these conclusions and can mimic the kinetic and steady state behavior of *mslo* macroscopic currents. In previous work, we proposed a general kinetic scheme for the gating of the *mslo* channel (Cui et al., 1997). Here we demonstrate how this scheme is a simplification of a more complex scheme based on sim-

Address correspondence to Dr. Richard W. Aldrich, Department of Molecular and Cellular Physiology, Beckman Center B171, Stanford, CA 94305-5426. Fax: 415-725-4463; E-mail: raldrich@popserver.stanford.edu

ple assumptions about the structure of the channel. We describe the basic properties of models of the simplified form, and we examine their ability to mimic *mslo* macroscopic currents.

METHODS

Electrophysiology

All experiments were performed with the mbr5 clone of the mouse homologue of the *slo* gene (*mslo*), which was kindly provided by Dr. Larry Salkoff (Washington University School of Medicine, St. Louis, MO). mbr5 cRNAs were expressed in *Xenopus laevis* oocytes and recordings were made in the inside-out patch clamp configuration from excised membrane patches as described previously (Cox et al., 1997). The solution in the recording pipette contained the following (mM): 140 $KMeSO_3$, 20 HEPES, 2 KCl, and 2 $MgCl_2$, pH 7.20. Internal solutions were prepared as described previously (Cox et al., 1997) and contained the following (mM): 140 $KMeSO_3$, 20 HEPES, 2 KCl, 1 HEDTA, and $CaCl_2$ to give the indicated free Ca^{2+} concentrations ([Ca]), pH 7.20. Final free Ca^{2+} concentrations ([Ca]) were determined with a Ca-sensitive electrode. HEDTA was not included in the internal solutions, which contained 490 and 1,000 μM [Ca]. 1 mM EGTA was substituted for HEDTA and no $CaCl_2$ was added to the internal solution containing ~2 nM [Ca]. At this [Ca], *mslo* channels can be activated by depolarization without binding Ca^{2+} (Meera et al., 1996; Cui et al., 1997). Solutions bathing the cytoplasmic face of the excised patch were exchanged using a sewer pipe flow system (DAD 12; Adams and List Associates Ltd., Westbury, NY) as described previously (Cox et al., 1997). Unless otherwise indicated, all currents were filtered at 10 kHz with a four pole low pass Bessel filter. Experiments were performed at 23°C. G-V relations were determined from the amplitude of tail currents 200 μs after repolarization to a fixed membrane potential (−80 mV) after 20-ms voltage steps to the indicated test voltages. Each *mslo* G-V relation was fitted with a Boltzmann function ($G = G_{max}/(1 + e^{zF(V_{1/2} - V)/RT})$) and normalized to the peak of the fit. The procedures used for the recording and analysis of *mslo* macroscopic currents minimized problems with permeation-related artifacts (see Cox et al., 1997).

Modeling

Voltage-dependent Monod-Wyman-Changeux (MWC)[1] models were fitted to *mslo* conductance voltage (G-V) relations at several [Ca] simultaneously using Eq. 5 and Table-Curve 3D software that employs an 80-bit Levenburg-Marquardt algorithm (Jandel Scientific, San Rafael, CA). Paramater standard errors were estimated by the curve-fitting algorithm. Similar fits were also found by eye. Parameters from fits to the steady state data constrained the rate constants used in fitting the kinetic data. The best over all steady state parameters were chosen as those that allowed for the best subsequent fit to the kinetic data. Four free parameters were involved in fitting voltage-dependent MWC models to the *mslo* G-V data. *mslo* G-V data were fitted to the general form of scheme II using Eqs. 2 and 3 and to two-tiered Koshland-Nemethy-Filmer (KNF) models using the following equation:

$$P_{open} = 1/1 + \left[\frac{1 + \frac{4[Ca]}{K_{CA}} + \frac{4[Ca]^2}{K_{CA}K_{CB}} + \frac{2[Ca]^2}{K_{CA}^2} + \frac{4[Ca]^3}{K_{CA}K_{CB}^2} + \frac{[Ca]^4}{K_{CB}^4}}{1 + \frac{4[Ca]}{K_{OA}} + \frac{4[Ca]^2}{K_{OA}K_{OB}} + \frac{2[Ca]^2}{K_{OA}^2} + \frac{4[Ca]^3}{K_{OA}K_{OB}^2} + \frac{[Ca]^4}{K_{OB}^4}}\right] L(0)\, e^{\frac{-QFV}{RT}} \quad (1)$$

To fit the macrosopic relaxation kinetics of *mslo* with voltage-dependent MWC models, simulated currents were generated using "Big Channel" kinetic modeling software written by Dr. Toshi Hoshi (University of Iowa, Iowa City, IA) and adapted to be compatible with "Igor Pro" curve fitting software (Wavemetrics Inc., Lake Osewgo, OR) by Dorothy Perkins (Howard Hughes Medical Institute, Stanford University). The activation and deactivation time courses of both real and model currents were then fitted with single exponential functions, and the time constants of these fits were compared. In both cases, fitting started 200 μs after initiation of the voltage step. Specific rate constants for fitting the model time constants to those of the *mslo* data were found by eye, but were aided by fitting to the relaxation time constants predicted by Eq. 9, which approximates the kinetic behavior of voltage-dependent MWC models under the conditions employed. Many of the rate constants of the models were constrained by the parameters determined from fitting the steady state data. To make the kinetic behavior of the models as exponential as possible, high Ca^{2+} binding rate constants were used. For each subunit, the Ca^{2+} binding rate constant was fixed at 10^9 $M^{-1}s^{-1}$ in both open and closed conformations. With this restriction, fitting the *mslo* kinetic data with voltage-dependent MWC models involved 10 free parameters. The general form of scheme II (see Fig. 3 *A*) was fit to the kinetic data of patch 1 in the same manner as was the voltage-dependent MWC model. For each subunit, the Ca^{2+} binding rate constant was fixed at 10^9 $M^{-1}s^{-1}$ in both closed and open conformations. Ca^{2+} unbinding rate constants were then determined from fits to the G-V data, and vertical rate constants were found by eye with the aid of Eq. 9. Fitting the *mslo* kinetic data to the general form of scheme II (see Fig. 3 *A*) involved 16 free parameters.

Statistical comparisons between voltage-dependent MWC, two-tiered KNF and general 10-state models were performed as described by Horn (1987). The statistic T, defined as

$$T = \frac{(SSE_f - SSE_g)}{SSE_g} \cdot \frac{(n - k_g)}{k_f},$$

was calculated and compared with the F distribution with k_f and $n - k_g$ degrees of freedom at the desired level of significance. Here, SSE_f represents the residual sum-of-squares for the fit with model f, which is a subhypothesis of model g; SSE_g represents the residual sum-of-squares for the parent model g, n represents the number of data points, and k_f and k_g represent the number of free parameters in models f and g, respectively.

The data from three representative patches were fitted independently (see Tables I, II, and III). For each of theses patchs, steady state and activation kinetic data were recorded at 8 or 9 [Ca] and at a large number of membrane voltages. Data from 19 additional patches recorded over more limited ranges of [Ca] and voltage behaved similarly. To increase the signal to noise ratio, typically four current families were recorded consecutively under identical conditions and averaged before analysis and display. Due to the long times necessary to acquire these data from a single patch deactivation, voltage families at a sufficiently large

[1]*Abbreviations used in this paper*: CNG, cyclic nucleotide–gated; KNF, Koshland-Nemethy-Filmer; MWC, Monod-Wyman-Changeux.

number of [Ca] were recorded only from patch 1. In fitting patches 2 and 3, the deactivation kinetics of patch 1 were used to constrain the kinetic fitting.

RESULTS

For simplicity, in modeling *mslo* macroscopic currents we have made the following assumptions about the structure of the channel.

(a) When expressed alone, mslo α subunits form homotetrameric channels. The work of Shen et al. (1994) supports this assumption. When they coexpressed mutant and wild-type *dslo* RNAs in *Xenopus* oocytes, they observed four different channel phenotypes at the single channel level that might reasonably correspond to channels with either zero, one, two, or three mutant subunits if each of four subunits contribute equally to the free energy of TEA binding. Also, over the first ~1/3 of their sequence, a region that includes the putative pore region, *slo* channels are structurally homologous to homotetrameric K^+ channels (Atkinson et al., 1991; Adelman et al., 1992; Butler et al., 1993; Tseng-Crank et al., 1994; McCobb et al., 1995).

(b) Each mslo α subunit contains a single Ca^{2+} binding site. There are many reports of Hill coefficients for Ca^{2+} activation >2.0 for both native and cloned BK channels (see McManus, 1991 and references given in INTRODUCTION) indicating that at least three Ca^{2+} binding sites contribute to channel activation. We have observed Hill coefficients >2.0 for the *mslo* channel as well (Cui et al., 1997). Given that the Hill coefficient in all but the most extremely cooperative case represents an underestimate of the true number of binding sites, and that the channel is likely to be a homotetramer, it seems reasonable to suppose that the channel has four Ca^{2+} binding sites, one on each subunit. However, we can not rule out more than four, particularly considering reports of Hill coefficients >4 for skeletal muscle BK channels in the presence of millimolar internal Mg^{2+} (Golowasch et al., 1986; Oberhauser et al., 1988).

(c) Each mslo α subunit contains a single voltage-sensing element. Supporting this assumption, each *mslo* α subunit has a partially charged putative membrane spanning region (S4), whose counterparts in purely voltage-gated K^+ channels are thought to form, at least in part, each of four voltage-sensing elements (Liman et al., 1991; Lopez et al., 1991; Papazian et al., 1991; Logothetis et al., 1993; Sigworth, 1994; Yang and Horn, 1995; Aggarwal and MacKinnon, 1996; Larsson et al., 1996; Mannuzzu et al., 1996; Seoh et al., 1996; Yang et al., 1996). Also, certain properties of the voltage dependence of *mslo* macroscopic and gating currents suggest that the channel multimer can undergo more than one voltage-dependent conformational change (see Horrigan et al., 1996; Ottolia et al., 1996; Toro et al., 1996; Cui et al., 1997, and DISCUSSION). It is possible, however, that each subunit can undergo more than one voltage-dependent conformational change. If this is the case, the main conclusions of this paper are not affected.

Assumptions *b* and *c* allow us to consider each subunit of the *mslo* channel as being able to reside in four physically distinct conformational states (Fig. 1 *A*): (*a*) Ca^{2+} bound, (*b*) voltage activated, (*c*) both Ca^{2+} bound and voltage activated, and (*d*) neither Ca^{2+} bound nor voltage activated. A channel comprised of four subunits (assumption *a*) then could reside in 4^4 or 256 states. However, without β subunit expression, each of *mslo*'s subunits are identical. Some of these states will not be physically distinct. How many are redundant will depend upon the symmetry of the tetramer. If the channel were to have twofold rotational symmetry such as is shown in Fig. 1 *B*, then it could occupy 73 physically distinct states. Several crystallized tetrameric proteins have been found to display this sort of symmetry (Dittrich, 1992). However, the *mslo* channel is thought to have a single pore, and its homology with *shaker* K^+ channels suggests that the same portion of each subunit contributes to the pore's structure (MacKinnon, 1991; Heginbotham and MacKinnon, 1992; MacKinnon et al., 1993). It is more likely, therefore, that the channel has fourfold rotational symmetry (Fig. 1 *C*). If this is the case, then there are 55 distinct channel states. These states are represented schematically in Fig. 2 *A*. Those states with a common number of bound Ca^{2+} are grouped. Notice that to be true to the physical picture (fourfold rotational symmetry), a distinction must be made between a channel with two Ca^{2+} bound to adjacent subunits and two Ca^{2+} bound to subunits, one diagonally across from the other. Similarly, there is a natural distinction between a channel with two voltage sensors activated in adjacent as opposed to diagonally opposite subunits. If the *mslo* channel exists as a homotetramer with a single Ca^{2+} binding site and a single voltage sensor in each subunit, then the states displayed in Fig. 2 *A* represent the smallest number that must be considered to describe the gating of the channel accurately.

Working with a 55-state kinetic model poses problems. First, due to the large number of equations necessary to represent such systems mathematically, testing them can be slow. Second, if there are energetic interactions between subunits (conclusion *e*, INTRODUCTION), then the number of parameters necessary to define the system's behavior can be very large, far larger than can be constrained by our data. And third, large kinetic models tend to lose their explanatory power as the system grows more complex. Even if one is able to find parameters by which a highly complex model fits the data well, it may not be easy to discern from these parameters why the model behaves as it does. For these reasons, we have taken two further steps to reduce the

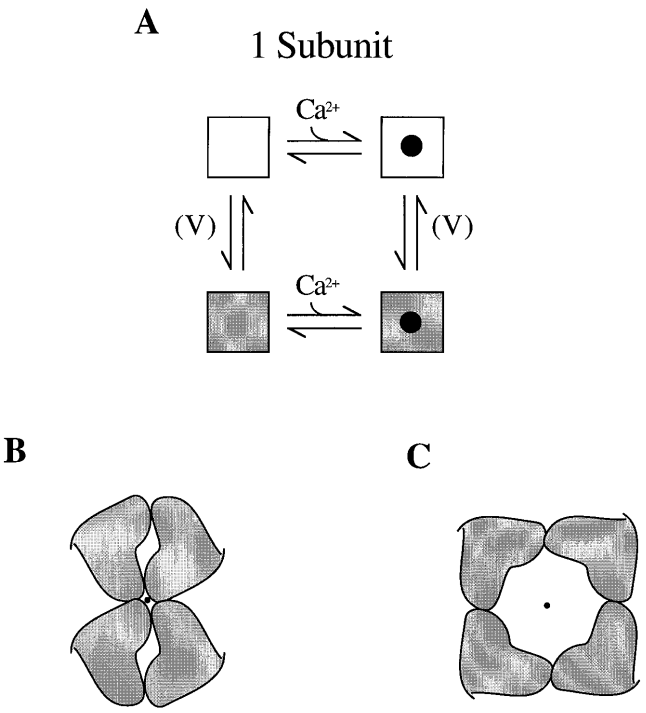

FIGURE 1. (*A*) Schematic representation of the four states of a channel subunit, which follow from assumptions 2 and 3. The filled circles represent the binding of a Ca^{2+} ion. The change in color from white to grey represents a voltage-dependent conformational change. These conventions are also followed in Figs. 2 and 3. (*B*) Illustration of an arrangement of four identical subunits that have twofold rotational symmetry about an axis perpendicular to the page passing through the point represented by the black dot. (*C*) Illustration of an arrangement of four identical subunits that have fourfold rotational symmetry about an axis perpendicular to the page passing through the point represented by the black dot.

number of kinetic states in the *mlso* model before trying to examine its performance. In doing so, however, we are aware that in terms of the idea represented in Figs. 1 *A* and 2 *A* we are over simplifying the system and may lose the ability to mimic certain important channel behaviors.

The first simplification is to make no distinction between two voltage- or Ca^{2+}-activated subunits that are adjacent to one another and two voltage- or Ca^{2+}-activated subunits diagonally opposed to one another. Examples of equivalent states under this assumption are shown in Fig. 2 *B*. The total number of conformations the channel may reside in then reduces to the 35 shown in Fig. 2 *C* (scheme I). Horizontal transitions represent Ca^{2+} binding and unbinding steps. Vertical transitions represent the movement of voltage-sensing elements. The states in each vertical grouping have a common number of Ca^{2+} ions bound. To avoid confusion, most of the allowable horizontal transitions are not represented; however, at all voltages the channel must bind four Ca^{2+} ions (undergo four horizontal transitions) to move from the leftmost column of states to the rightmost column.

To use scheme I to model channel gating, each state must be designated as open or closed. The states in the uppermost tier (*horizontal row*) may be designated closed, as even at high Ca^{2+} concentrations strong hyperpolarization reduces the channel's open probability to very low levels (Latorre et al., 1982; Moczydlowski and Latorre, 1983; Adelman et al., 1992; Wei et al., 1994; DiChiara and Reinhart, 1995; Cox et al., 1997; Cui et al., 1997). The states in the lowermost tier may be designated open, as strong depolarization can bring the *mslo* channel to very high open probabilities (>0.9) with or without bound Ca^{2+} (Cox et al., 1997; Cui et al., 1997). Which intermediate states (those inside the box in Fig. 2 *C*) are open is not obvious. Bearing on this issue, the *mslo* G-V relation can be approximated by a simple Boltzmann function over a wide range of Ca^{2+} concentrations (Butler et al., 1993; Wei et al., 1994; Cui et al., 1997),[2] and simulations indicate that for scheme I to predict Boltzmann-like G-V relations, the voltage-dependent transitions that link the uppermost closed tier to the lowermost open tier must be highly concerted. By concerted we mean that the change in standard free energy associated with the last gating step before opening is much larger than the previous steps such that the probability of the channel occupying an intermediate state at equilibrium is low at most Ca^{2+} concentrations and membrane voltages (conclusion *e* in INTRODUCTION). If this is the case, we can approximate scheme I by scheme II, shown in Fig. 3 *A*. Here the four voltage-dependent steps in scheme I are represented by a single, and therefore completely concerted, voltage-dependent step. Which intermediate states are open is no longer an issue. Further suggesting that there is a single conformational change that is limiting the rate of current relaxations under most circumstances (see below), macroscopic *mslo* kinetics are nearly exponential over a wide range of Ca^{2+} concentrations and membrane voltages (see Fig. 9 and Cui et al., 1997). Condensation of intermediate voltage-dependent steps to a single step, therefore, at least as a first approximation, may be reasonable, although departures from strictly single exponential behavior are known (Toro et al., 1996; Cui et al., 1997).

The hypothesis represented by scheme II may be described as follows. The channel can exist in two main conformations, closed and open. The equilibrium between closed and open is voltage dependent, having associated with it a gating charge Q. The channel has four identical Ca^{2+} binding sites, and the binding of

[2]Although a single Boltzmann function often appears to fit the data well, somewhat better fits can be achieved by fitting to a Boltzmann function raised to a power >1 (Cui et al., 1997).

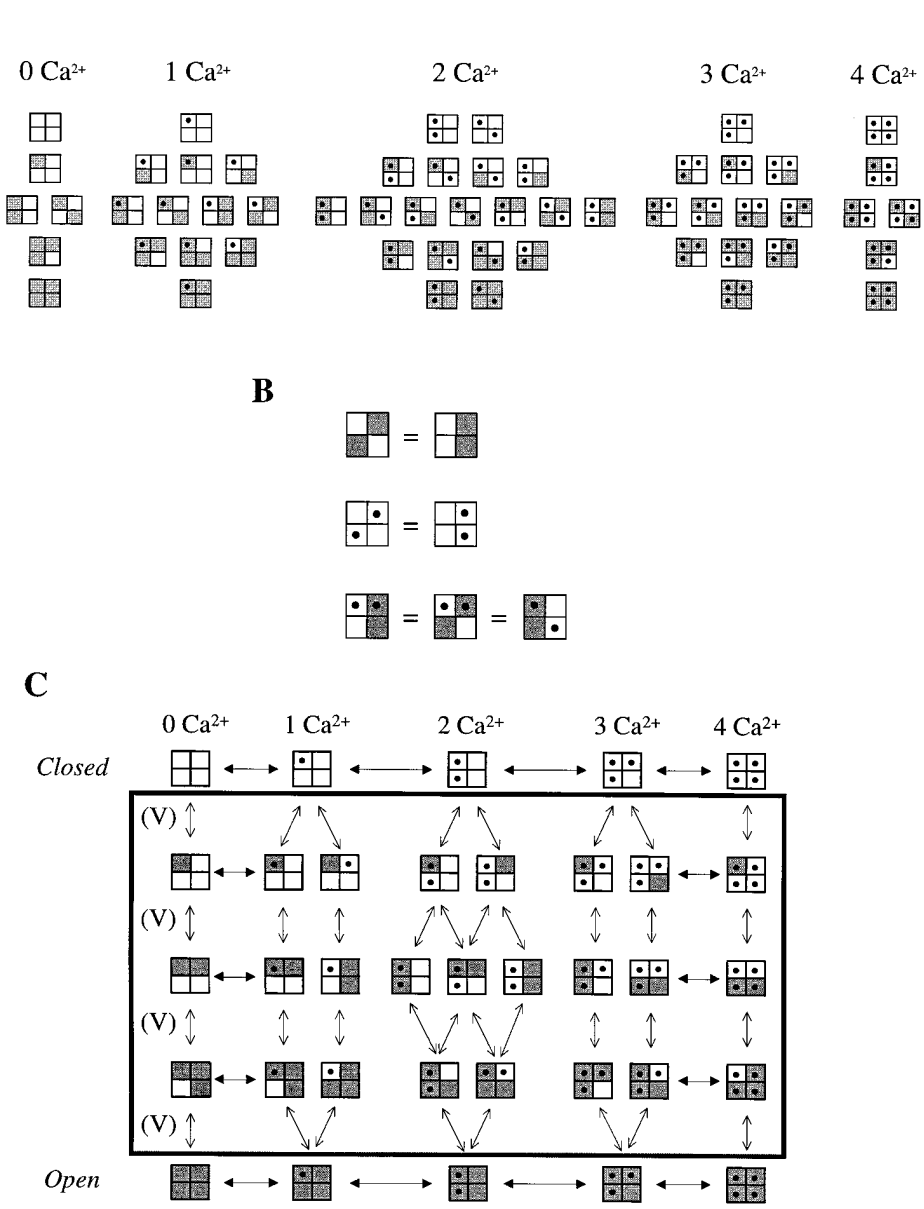

SCHEME I

FIGURE 2. (*A*) Schematic representation of the 55 states of a fourfold symmetric homotetrameric channel that follow from the state diagram for each subunit in Fig. 1 *A*. These states, as well the 73 physically distinct states that a twofold symmetric homotetrameric channel can occupy (not shown), were found by enumeration. Each grouping of states represents those with a different number of Ca^{2+} ions bound as indicated. (*B*) Illustration of some equivalent states when no distinction is made between two activated subunits adjacent to one another and two activated subunits diagonally opposed to one another. (*C*) Scheme I, 35-state channel gating scheme that follows from assumptions 1, 2, and 3 if the simplifying assumption illustrated in *B* is made. In general, when subunit position is not taken into consideration, the number of states of a homomultimer with r subunits, each subunit of which can exist in n states, is given by the binomial coefficient $(n + r - 1: n - 1)$ (Feller, 1968). Horizontal arrows represent Ca^{2+} binding steps. For simplicity, not all horizontal steps are represented. Each vertical grouping includes states with a given number of bound Ca^{2+} as indicated. Each horizontal tier represents a different number of activated voltage sensors.

Ca^{2+} shifts the closed-to-open equilibrium towards open. The simplest physical picture that corresponds to scheme II is one in which, in either of the two main conformations of the protein, the Ca^{2+} binding sites act independently. The binding of one Ca^{2+} ion does not influence the binding of subsequent Ca^{2+} to that same conformation; only undergoing the closed-to-open conformational change affects Ca^{2+} binding affinity, and then all sites are affected equally. In this case, scheme II corresponds to a voltage-dependent version of the Monod-Wyman-Changeaux model originally proposed to describe the binding of oxygen to hemoglobin (Monod et al., 1965). Here, the usual R and T nomenclature is replaced by O and C, and the central conformational change is made voltage dependent. MWC models have been used to describe the equilibrium behavior of many of the best studied allosteric proteins (Dittrich, 1992), particularly tetrameric proteins: hemoglobin, phosphofructokinase, and fructose-1,6-bisphosphatase for example. However, unlike in the study of most allosteric proteins, in studying channel gating we are better able to measure the fraction of channels in the R, or open state, than the fraction of binding sites occupied by ligand. Nevertheless, the fact that an examination of

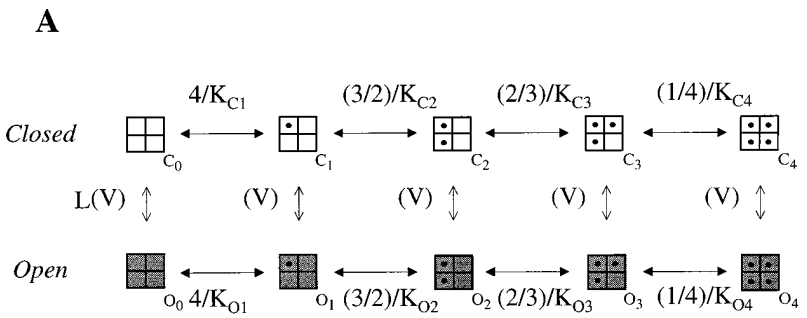

SCHEME II

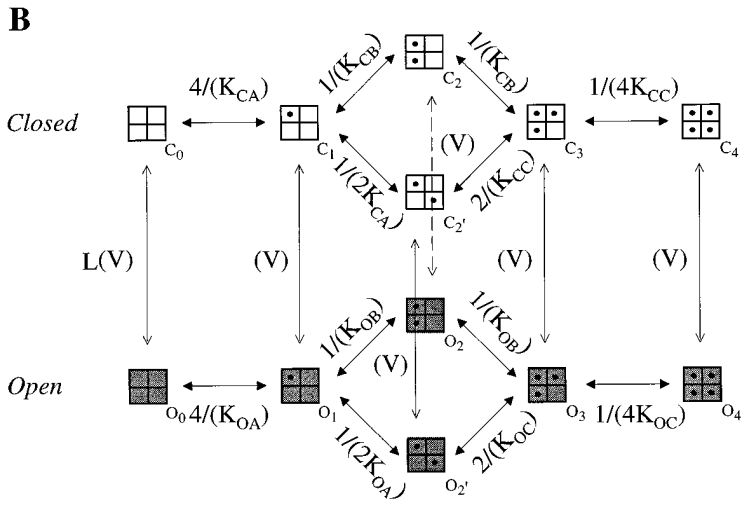

SCHEME III

FIGURE 3. (*A*) Scheme II, two-tiered gating scheme that follows from scheme I if it is supposed that the voltage sensors from each subunit move in a highly concerted way such that their movement can be represented by a single voltage-dependent conformational change. This scheme is derived from scheme I by eliminating the states in the black box in Fig. 2 *C*. Those states in the upper tier are designated closed. Those states in the lower tier are designated open. K_{C1}, K_{C2}, K_{C3}, K_{C4} represent Ca^{2+} dissociation constants in the closed conformation. K_{O1}, K_{O2}, K_{O3}, K_{O4} represent Ca^{2+} dissociation constants in the open conformation. When $K_{C1} = K_{C2} = K_{C3} = K_{C4}$ and $K_{O1} = K_{O2} = K_{O3} = K_{O4}$, scheme II represents a voltage-dependent version of the Monod-Wyman-Changeaux model of allosteric proteins (Monod et al., 1965). (*B*) Scheme III, two-tiered KNF model. The binding of Ca^{2+} to each tier is supposed to affect the dissociation constants of the sites on adjacent subunits. K_{CA} represents the dissociation constant of a subunit with no neighbors occupied, K_{CB} represents the dissociation constant of a subunit with one neighbor occupied. K_{CC} represents the dissociation constant of a subunit with two neighbors occupied and is determined by K_{CB}^2/K_{CA}. K_{OA}, K_{OB}, and K_{OC} are similarly defined for the open tier.

the gating behavior of *mslo* leads to models of the form of scheme II suggests that perhaps this channel has something mechanistically in common with these other allosteric proteins. As described below, we examined the ability of voltage-dependent MWC models to predict the macroscopic behavior of *mslo* channels. In addition, we have examined the general characteristics of models that do not conform to the MWC constraint that each binding site acts independently but are of the form of scheme II.

mslo Steady State Behavior

Assuming that Ca^{2+} binding is not voltage dependent (see Cui et al., 1997), the equilibrium open probability (P_{open}) of models of the form of scheme II can be written as the following function of [Ca] and voltage:

$$P_{open} = \frac{1}{1 + \left[\frac{\frac{[Ca]^4}{K_{C1}K_{C2}K_{C3}K_{C4}} + \frac{4[Ca]^3}{K_{C1}K_{C2}K_{C3}} + \frac{6[Ca]^2}{K_{C1}K_{C2}} + \frac{4[Ca]}{K_{C1}} + 1}{\frac{[Ca]^4}{K_{O1}K_{O2}K_{O3}K_{O4}} + \frac{4[Ca]^3}{K_{O1}K_{O2}K_{O3}} + \frac{6[Ca]^2}{K_{O1}K_{O2}} + \frac{4[Ca]}{K_{O1}} + 1} \right] L(V)} \quad (2)$$

where K_{Ci} is the dissociation constant for the subunit binding the ith Ca^{2+} in the closed conformation, K_{Oi} is the dissociation constant for the subunit binding the ith Ca^{2+} in the open conformation, and L(V) is the open-to-closed equilibrium constant ($[C_0]/[O_0]$) when no Ca^{2+} ions are bound to the channel. If we assume that the free energy of the channel varies linearly with voltage, as is likely to be the case at moderate voltages (Stevens, 1978), then L(V) can be defined as:

$$L(\mathrm{V}) = L(0)\, e^{\frac{-QFV}{RT}} \tag{3}$$

where, F is Faraday's constant, R is the universal gas constant, T is temperature, V is voltage, and Q is the equivalent gating charge associated with the closed-to-open conformational change, and $L(0)$ is the open-to-closed equilibrium constant in the absence of bound Ca^{2+} at 0 mV. Combining Eqs. 2 and 3, P_{open} depends on voltage in the form of a Boltzmann function:

$$P_{\mathrm{open}} = \frac{1}{1 + BL(0)\, e^{\frac{-QFV}{RT}}} \tag{4a}$$

with

$$B = \left[\frac{\frac{[\mathrm{Ca}]^4}{K_{C1}K_{C2}K_{C3}K_{C4}} + \frac{4[\mathrm{Ca}]^3}{K_{C1}K_{C2}K_{C3}} + \frac{6[\mathrm{Ca}]^2}{K_{C1}K_{C2}} + \frac{4[\mathrm{Ca}]}{K_{C1}} + 1}{\frac{[\mathrm{Ca}]^4}{K_{O1}K_{O2}K_{O3}K_{O4}} + \frac{4[\mathrm{Ca}]^3}{K_{O1}K_{O2}K_{O3}} + \frac{6[\mathrm{Ca}]^2}{K_{O1}K_{O2}} + \frac{4[\mathrm{Ca}]}{K_{O1}} + 1} \right] \tag{4b}$$

The steepness of this relation as a function of V is determined solely by the value of Q, and is therefore independent of [Ca]. Assuming no voltage dependence in Ca^{2+} binding, models of the form of scheme II will predict a G-V that does not change shape as [Ca] is varied. The position of the G-V curve on the voltage axis, however, will be determined by $BL(0)$, and therefore will depend on $L(0)$, [Ca], and all the Ca^{2+} dissociation constants for both the closed and open channel. For voltage-dependent MWC models, where the microscopic dissociation constants depend only on whether the channel is open or closed, Eq. 4 simplifies to

$$P_{\mathrm{open}} = \frac{1}{1 + \left[\frac{(1 + \frac{[\mathrm{Ca}]}{K_C})}{(1 + \frac{[\mathrm{Ca}]}{K_O})} \right]^4 L(0)\, e^{\frac{-QFV}{RT}}} \tag{5}$$

Shown in each panel of Fig. 4 are data from 22 macropatches expressing *mslo* channels. These patches were excised from *Xenopus* oocytes and superfused with solutions of varying [Ca]. Each data point represents the half maximal activation voltage ($V_{1/2}$) of the ionic current in a particular patch at the indicated [Ca]. At each [Ca], typically three to five current families were recorded and averaged before analysis. In three experiments, it was possible to expose the patch to eight or more Ca^{2+} concentrations and determine complete G-V relations. The $V_{1/2}$ values from these patches are indicated as filled circles in Fig. 4. (patch 1, Fig. 4 *A*; patch 2, Fig. 4 *B*; patch 3, Fig. 4 *C*), and the full G-V relations from these patches are shown in Fig. 5. Also

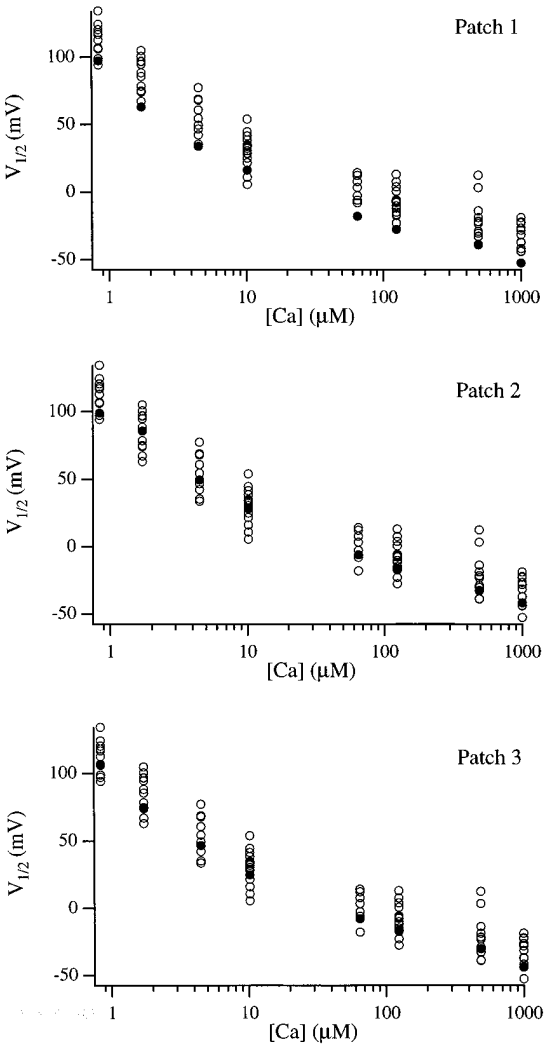

FIGURE 4. $V_{1/2}$ vs. [Ca] plots highlighting the three patches displayed in Fig. 5. Each data point represents the voltage at which the *mslo* G-V relation reached half maximal activation at the indicated [Ca]. In *A–C*, the data are from the same 22 patches; however, in *A* the $V_{1/2}$ values for patch 1 (Fig. 5) are darkened, in *B* the $V_{1/2}$ values for patch 2 (Fig. 5) are darkened, and in *C* the $V_{1/2}$ values for patch 3 (Fig. 5) are darkened.

shown in Fig. 5 are voltage-dependent MWC model fits to these data (*solid lines*) using Eq. 5.

The fits to each set of G-V curves are determined by four parameters: the closed Ca^{2+} dissociation constant (K_C), the open Ca^{2+} dissociation constant (K_O), and, as already defined, $L(0)$ and Q. Voltage-dependent MWC models can fairly well describe the *mslo* G-V relation at very low [Ca] (Fig. 5, *A* and *B*, *open circles*), as well as the shifting behavior of the G-V relation as Ca^{2+} is increased to 124 μM. The calculated G-V curves displayed in bold correspond to the following [Ca]: ~2 nM, 0.84, 1.7, 4.5, 10.2, 65, and 124 μM. The best fitting parameters for each patch over this [Ca] range are listed in Table I. At higher [Ca] (dimmed data and fits), the *mslo*

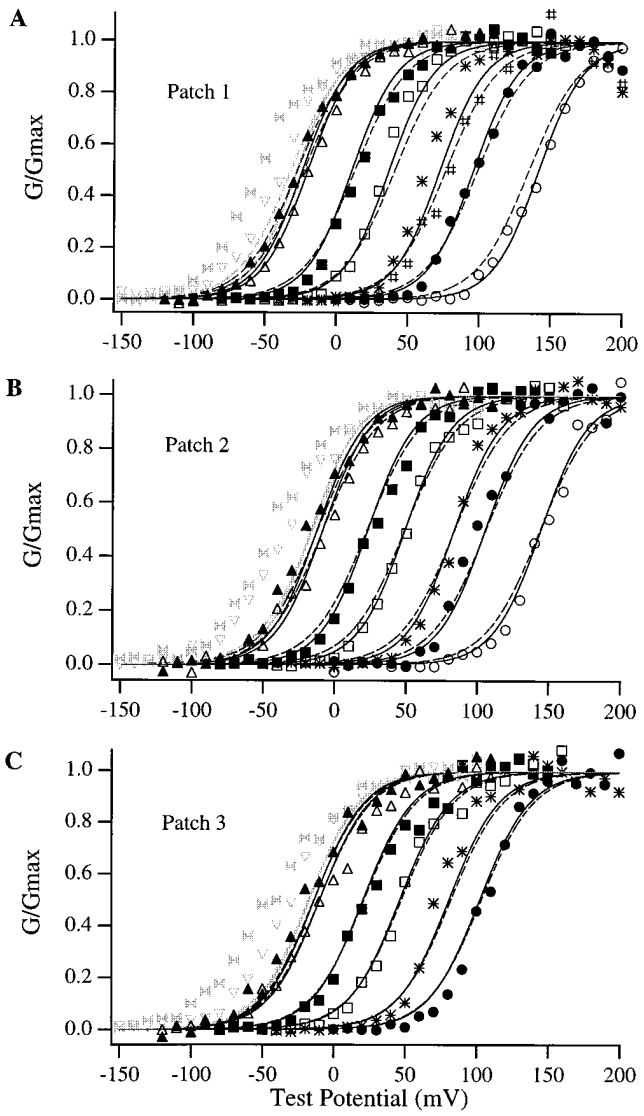

FIGURE 5. *mslo* G-V relations determined from macroscopic currents at the following [Ca]: ~2 nM (○), 0.84 (●), 1.7 (*), 4.5 (□), 10.2 (■), 65 (△), and 124 μM (▲). Data from three patches are displayed (*A–C*). Solid lines represent best least squares voltage-dependent MWC model fits to these data over the [Ca] range ~2 nM–124 μM. Parameters for these fits are listed in Table I. The dashed lines represent best overall MWC model fits taking into account both kinetic and steady state data. Parameters for these fits were found by eye and are listed in Table III. Two sets of data recorded with 1.7 μM [Ca] are displayed in *A* corresponding to the beginning (*) and end (#) of this ~40-min experiment. The grey symbols are data from 490 (▽), and 1,000 μM (▶◀) [Ca]. Model fits to these data are also included (*grey solid and dashed lines*). Patch 1 contained ~100 channels. Patch 2 contained ~70 channels. Patch 3 contained ~80 channels. Similar data from patch 2 were displayed in Cui et al. (1997; Fig. 5 *A*). Typically, three or four voltage families were recorded consecutively and averaged before analysis.

G-V relation is not well fitted by voltage-dependent MWC models. Possible reasons for this discrepancy will be considered later in some detail. Two G-V relations recorded with 1.7 μM [Ca] are included in Fig. 5 *A*, one recorded at the beginning of this ~40-min experiment and the other recorded at the end. The difference between these two data sets reflects the variability in G-V position over time, and therefore provides some assessment of how accurately we might expect the model to fit the steady state data if it were known a priori that such a model properly mimicked the underlying physical system. Given this variability, the model appears to mimic *mslo* steady state behavior over the [Ca] range ~2 nM–124 μM fairly well.

In some previous experiments, however, at very low [Ca] (~0.5 nM), the maximum slope of the *mslo* G-V relation was more shallow than that observed at ~2 nM [Ca] for patches 1 and 2 in Fig. 5, (mean Boltzmann fit parameters: z = 0.87, $V_{1/2}$ = 195 mV, ~0.5 nM [Ca], Cui et al., 1997), and it was more shallow than its value at 10.2 μM [Ca] by ~30% (Cui et al., 1997). Also, some variation in G-V curve steepness is observed throughout the [Ca] range. On average, we have found this relation to be most steep at ~2 μM [Ca], and to become somewhat more shallow at both higher and lower [Ca] (Cui et al., 1997). For voltage-depedendent MWC models, the value of Q determines the G-V relations steepness, and, supposing there is no voltage dependence in horizontal transitions, dictates that the model G-V relation will have the same shape regardless of [Ca] (see Fig. 6 for example). Variations in G-V curve shape as a function of [Ca], therefore, cannot be accounted for by these simplified models. Models of the form of scheme I, however, could likely account for this behavior as scheme I allows for differences in the cooperative interactions between voltage sensing elements when different numbers of Ca^{2+} are bound to the channel. Alternatively, adding a small amount of voltage dependence to the Ca^{2+} binding steps in scheme II, or assigning a nonexponential voltage dependence to the central closed-to-open conformational change can also give rise to changes in G-V curve steepness as [Ca] is varied.

Properties of Scheme II Models

In Fig. 4 we used the voltage at which *mslo* currents are half maximally activated ($V_{1/2}$) as an index of the position of the channel's G-V relation on the voltage axis at a given [Ca]. In the study of BK channel gating, this is common practice (Wong et al., 1982; Wei et al., 1994; DiChiara and Reinhart, 1995; McManus et al., 1995; Wallner et al., 1995; Dworetzky et al., 1996; Meera et al., 1996; Cui et al., 1997). For models conforming to scheme II

$$V_{1/2} = \frac{RT}{QF} ln(BL(0)) \quad (6)$$

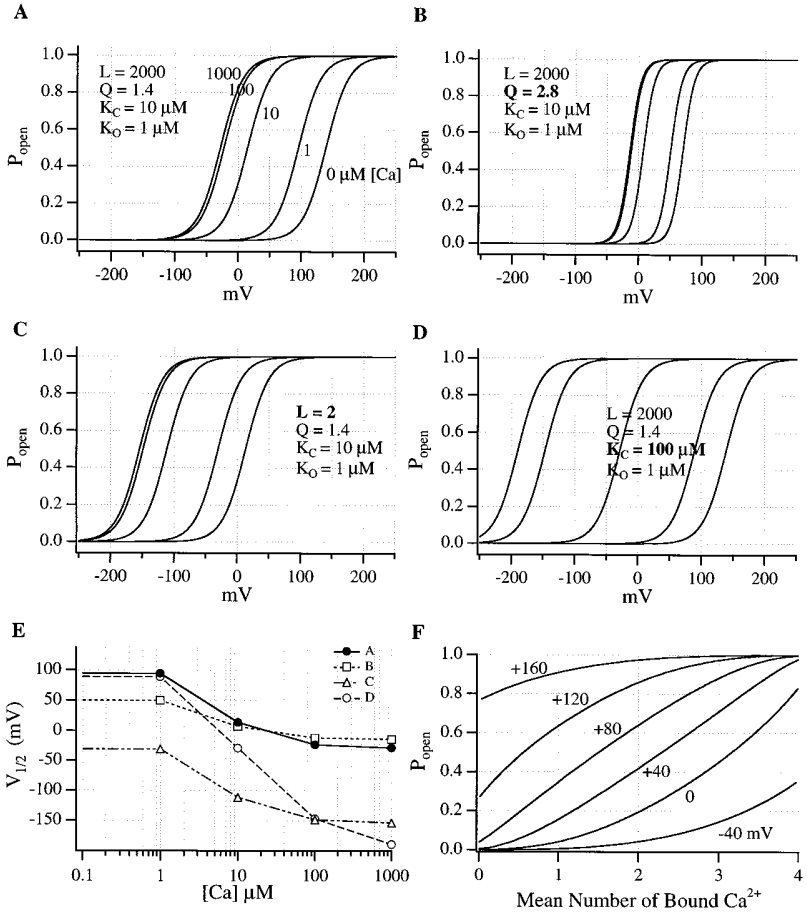

FIGURE 6. Equilibrium behavior of voltage-dependent MWC models. (*A*) Model G-V curves at 0, 1, 10, 100, and 1,000 µM [Ca]. The parameters used to generate these curves are indicated on the figure, and are similar to those used to fit the *mslo* data in Fig. 5 (Table III). (*B*) The effects of changing Q from 1.4 to 2.8. (*C*) The effects of changing $L(0)$ from 2,000 to 2. (*D*) The effects of changing K_C from 10 to 100 µM. (*E*) Plots of $V_{1/2}$ vs. log[Ca] for the conditions indicated in *A* (●), *B* (□), *C* (△), and *D* (○). (*F*) At higher voltages, fewer bound Ca^{2+} are necessary to achieve a given level of open probability. Plotted is open probability (P_{open}) as a function of the mean number of Ca^{2+} ions bound to the model channel. Each curve represents a different voltage as indicated. Model parameters were the same as in *A*. Open probability was calculated from Eq. 5. The mean number of Ca^{2+} ions bound to the model channel (*M*) was calculated from the relation $M = 4(L(K_O/K_C)([Ca]/K_O)(1 + [Ca]/K_C)^3 + ([Ca]/K_O)(1 + [Ca]/K_O)^3)/(L(1 + [Ca]/K_C)^4 + (1 + [Ca]/K_O)^4)$ where L is given by Eq. 3.

where B is given by Eq. 4*b*, and is thus a function of [Ca] and its dissociation constants. At constant Q and [Ca], a decrease in $L(0)$ decreases the change in free energy required to open the channel, and the G-V relation moves leftward along the voltage axis. If $L(0)$ and [Ca] are held constant and Q is increased, more energy is imparted to the central equilibrium by a given change in voltage, and $V_{1/2}$ moves towards 0 mV. When [Ca] equals 0, B equals 1, and the position of the G-V relation is determined only by Q and $L(0)$. The effects that changes in various voltage-dependent MWC model parameters have on model G-V relations at a series of [Ca] are illustrated in Fig. 6.

The parameters that best fit the *mslo* G-V data (Table I) suggest an intrinsic standard free energy difference between open and closed at 0 mV of 4.6–5.4 kcal mol^{-1} at 23°C. However, the standard errors of estimates of $L(0)$ are large. The $L(0)$ values could be further constrained by fits to kinetic measurements of gating. Smaller values of Q, and therefore correspondingly smaller values of $L(0)$, could give similar fits to the *mslo* G-V relations (dashed lines in Fig. 5), and, as will be discussed, yielded better fits to the kinetic data. In fitting both steady state and kinetic data, therefore, lower values of $L(0)$ were favored. Typically, values of $L(0)$ between 1,500 and 2,000 were used (see Table III) corresponding to an intrinsic free energy difference between closed and open at 0 mV of 4.3–4.5 kcal mol^{-1} at 23°C.

Taking the derivative of Eq. 6 with respect to $L(0)$ yields:

$$\frac{dV_{1/2}}{dL(0)} = \frac{RT}{QFL(0)} \tag{7}$$

The Ca-dependent factor B in Eq. 6 does not appear in Eq. 7. Therefore, the effects of changing $L(0)$ are the same at each [Ca], and as $L(0)$ is varied, the G-V curves

TABLE I

Voltage-dependent MWC Model Parameters

	Steady state fitting		
Parameter	Patch 1	Patch 2	Patch 3
$L(0)$	8959 ± 2375*	6182 ± 1504	2497 ± 1015
Q	1.64 ± 0.04*e*	1.54 ± 0.04*e*	1.43 ± 0.05*e*
K_C	9.37 ± 0.50 µM	10.22 ± 0.52 µM	9.02 ± 0.72 µM
K_O	0.62 ± 0.03 µM	0.89 ± 0.05 µM	0.99 ± 0.13 µM

Parameters are from least squares fits over the [Ca] range ~2 nM–124 µM, patches 1 and 2; and 0.84–1,000 µM, patch 3. *Parameter standard error.

TABLE III

Voltage-dependent MWC Model Parameters

Parameter	Steady state and kinetic fitting		
	Patch 1	Patch 2	Patch 3
Steady state parameters*			
$L(0)$	1647	2029	1806
Q	1.40e	1.35e	1.37e
K_C	11.0 μM	8.68 μM	9.03 μM
K_O	1.1 μM	1.04 μM	1.08 μM
Kinetic parameters			
Vertical rate constants			
	Closed to open*		
$C_0 \rightarrow O_0$	2.39 s^{-1}	1.8 s^{-1}	2.0 s^{-1}
$C_1 \rightarrow O_1$	7.0 s^{-1}	5.5 s^{-1}	5.0 s^{-1}
$C_2 \rightarrow O_2$	40 s^{-1}	29 s^{-1}	38 s^{-1}
$C_3 \rightarrow O_3$	295 s^{-1}	130 s^{-1}	160 s^{-1}
$C_4 \rightarrow O_4$	557 s^{-1}	300 s^{-1}	340 s^{-1}
Charge	0.73e	0.71e	0.71e
	Open to closed		
$O_0 \rightarrow C_0$	3936 s^{-1}	3652 s^{-1}	3612 s^{-1}
$O_1 \rightarrow C_1$	1152 s^{-1}	1338 s^{-1}	1076 s^{-1}
$O_2 \rightarrow C_2$	659 s^{-1}	846 s^{-1}	974 s^{-1}
$O_3 \rightarrow C_3$	486 s^{-1}	490 s^{-1}	489 s^{-1}
$O_4 \rightarrow C_4$	92 s^{-1}	126 s^{-1}	124 s^{-1}
Charge	−0.67e	−0.64e	−0.66e
Horizontal rate constants			
Ca^{2+} on-rates equaled 10^9 $M^{-1}s^{-1}$* for each binding site in both open and closed channel conformations and were adjusted appropriately for the number of available sites.			
Ca^{2+} off-rates equaled ($10^9 K_C$) for each binding site in the closed conformation and ($10^9 K_O$) for each binding site in the open conformation, and were adjusted appropriately for the number of bound Ca^{2+}.			

*These parameters are sufficient to define the kinetic behavior of these models.

for a number of [Ca] move as a set along the voltage axis maintaining the spacing between them (compare Fig. 6, *C* to *A*). The shape of the $V_{1/2}$ vs. log[Ca] relation does not change (Fig. 6 *E*).

Unlike $L(0)$, the value of Q influences the spacing of the model G-V curves. For a given series of [Ca], increases in Q bring the model curves closer together (compare Fig. 6, *B* to *A*). This can be understood intuitively by considering that as the gating valence is increased the free energy contributed to the central conformational equilibrium by a given size electric field increases; therefore, smaller increases in the size of this field are required to compensate for the free energy contributed to this equilibrium by Ca^{2+} binding. It can also be understood mathematically by considering that Q appears in the denominator of Eq. 6. A large Q value will therefore mitigate the change in $V_{1/2}$ brought about by increases in [Ca]. The slope of the $V_{1/2}$ vs. log[Ca] relation becomes more shallow as Q is increased (Fig. 6 *E*). The relative spacing of the model G-V relations, however, which we might define as the difference in $V_{1/2}$ between the G-V curves for any two [Ca] divided by the difference in $V_{1/2}$ for any other two [Ca], is unaffected by changes in Q. This is a manifestation of the fact that a plot of $V_{1/2}$ vs. log[Ca] scales linearly with $(1/Q)$ (Eq. 6).

To this point, our analysis has been based on equations for the general form of scheme II. The effects described above are therefore not specific to voltage-dependent MWC models, but rather are general to all models of this form.

When Q and the number of binding sites are fixed, the spacing of the G-V curves along the voltage axis as [Ca] is varied is determined by all the Ca^{2+} dissociation constants in the system, K_C and K_O for voltage-dependent MWC models. These constants reflect the change in free energy that occurs as Ca^{2+} binds to either conformation of the protein, and their ratio determines the maximum shift in $V_{1/2}$ as [Ca] is increased from 0 to a saturating value. Comparing Fig. 6 *D* to *A* for example, as K_C is increased from 10 to 100 μM, the position of the model G-V relation at high [Ca] shifts considerably leftward due to an increase in the ratio K_C/K_O. Notice that this large leftward shift is accomplished by decreasing the affinity of the channel for Ca^{2+} in the closed state. Such shifts are therefore not necessarily indicative of an increase in Ca^{2+} binding affinity. The G-V relation at 0 [Ca], is unaffected. Within the range between 0 and saturating [Ca], the specific values of the Ca^{2+} dissociation constants determine the spacing of the G-V relations. In fitting *mslo* G-V relations to voltage-dependent MWC models, we consistently found that to create the observed spacing the values of K_C and K_O had to be close to 10 μM and 0.5–1 μM, respectively (see Table I for standard errors). In terms of these models, then, K_C and K_O are well determined.

Accounting for the mslo G-V Relation at High [Ca]

As is evident in Fig. 5, the position of the *mslo* G-V relation at very high [Ca] is not well accounted for by voltage-dependent MWC models. The dimmed data points in this figure were recorded with 490 (*triangles*) and 1,000 (*bowties*) μM [Ca]. Model fits are also shown (*gray lines*). Both real and model G-V relations are close together at 65 and 124 μM [Ca], suggesting a saturation of the effects of [Ca]. At higher [Ca], however, the *mslo* G-V curve continues to move leftward, while the model curve saturates. In fitting the data in Fig. 5, only the [Ca] range, ~2 nM–124 μM, was included and, therefore, good fits at higher [Ca] might not be expected. However, as shown in Fig. 7 *A*, when data recorded at 490 and 1,000 μM [Ca] are included in the fitting, voltage-dependent MWC models cannot account for the position of the G-V curves at the highest [Ca]. Attempting to do so sacrifices fitting the data at lower [Ca]. Increasing the number of Ca^{2+} binding sites did not im-

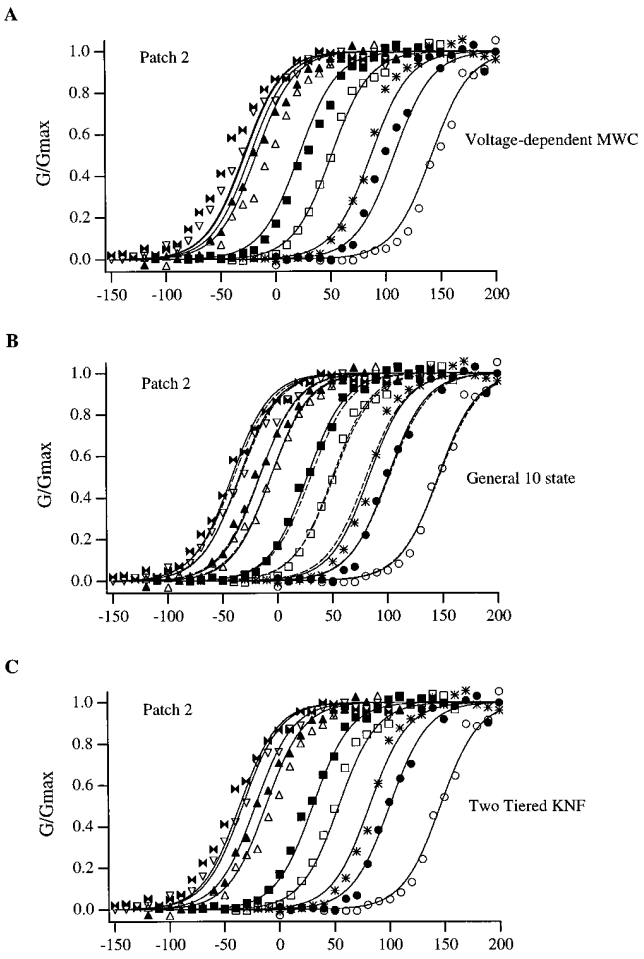

FIGURE 7. (*A*) Voltage-dependent MWC model, (*B*) general 10-state model, and (*C*) two-tiered KNF model least squares best fits to the steady state data of patch 2 (of Fig. 5), with data points at 490 and 1,000 μM included in the fitting. The parameters for the voltage-dependent MWC model fit are: K_C = 13.28 μM, K_O = 1.17 μM, $L(0)$ = 3,052.5, Q = 1.44*e*. The parameters for the least squares general 10-state model fit are listed in Table II. The parameters for the two-tiered KNF model fit are: K_{CA} = 0.046 μM, K_{CB} = 1.42 μM, K_{CC} = 43.90 μM, K_{OA} = 0.047 μM, K_{OB} = 0.100 μM, K_{OC} = 0.213 μM, Q = 1.46*e*, $L(0)$ = 4,328. The dashed lines in *B* represent a fit to the general 10-state model with the following parameters: K_{C1} = 9.03 μM, K_{C2} = 5.97 μM, K_{C3} = 5.90 μM, K_{C4} = 135.7 μM, K_{O1} = 0.68 μM, K_{O2} = 0.85 μM, K_{O3} = 1.19 μM, K_{O4} = 1.65 μM, Q = 1.38*e*, $L(0)$ = 2,882.5.

prove model fits at high [Ca]. For each patch, the residual sum of squares increased as the number of binding sites in the model was increased.

We also tried to fit the data at high [Ca] by relaxing the MWC constraint that there are no interactions between Ca^{2+} binding sites in either the closed or open channel. The affinity constants $K_{C1} - K_{C4}$ and $K_{O1} - K_{O4}$ in scheme II were allowed to vary independently. In physical terms, relaxation of this constraint allows each Ca^{2+} binding to affect the affinities of the remaining unoccupied sites. The sequential nature of each horizontal row in scheme II (Fig. 3 *A*), however, dictates that all unoccupied sites are affected equally by any binding event. As shown in Fig. 7 *B* (*solid lines*), relaxing the MWC independent binding constraint significantly improved model fits to the *mslo* G-V relations at high [Ca] ($P < 0.01$ for each patch, tests for the superiority of nested regression models where carried out as described by Horn, 1987, see METHODS). The general 10-state model parameters that best fit patch 2 in Fig. 7 *B* are listed in Table II, as are the parameters that best fit the G-V data from the two other patches in Fig. 5. The dissociation constants from these fits suggest a complex relationship between successive Ca^{2+} binding events in both the open and closed conformation. The standard errors of these fit parameters, however, were very large, sometimes several orders of magnitude larger than the parameter values themselves. This result suggests that many different parameter combinations could produce similar fits, and therefore no emphasis should be placed on any particular parameter combination. It also underscores the inadequecy of steady state data for constraining complex models, and the need for both steady state and kinetic data to obtain reliable parameter estimates.

A common property of each fit, however, is a large K_{C4} value relative to the other closed state Ca^{2+} dissociation constants. This decrease in the affinity of the last Ca^{2+} binding event in the closed conformation, coupled with no change or an increase in the affinity of the last Ca^{2+} binding event in the open conformation, increases the ratio (K_{C4}/K_{O4}) and thereby the power of the last binding event to push the G-V relation leftward along the voltage axis. This effect can account for most of the improvement over voltage-dependent MWC fits at high [Ca]. This is demonstrated by the dashed lines in Fig. 7 *B*, which represent a general 10-state model fit to these data with parameters that are similar to the

TABLE II
General 10-State Model Parameters

	Steady state fitting		
Parameter	Patch 1	Patch 2	Patch 3
$L(0)$	4865.3	3729.9	5896.7
Q	1.53*e*	1.42e	1.32*e*
K_{C1}	43.27 μM	26.10 μM	10.59 μM
K_{C2}	2.78 μM	18.55 μM	2.37 μM
K_{C3}	1.17 μM	0.94 μM	3.44 μM
K_{C4}	196.74 μM	204.72 μM	125.24 μM
K_{O1}	0.58 μM	0.31 μM	1.58 μM
K_{O2}	1.81 μM	7.39 μM	0.40 μM
K_{O3}	0.91 μM	0.82 μM	0.15 μM
K_{O4}	0.16 μM	0.70 μM	1.61 μM

Parameters are from least squares fits over the [Ca] range ~2 nM–1,000 μM, patches 1 and 2; and 0.84–1,000 μM, patch 3.

voltage-dependent MWC model parameters for this patch (Tables I and III), except for a large K_{C4} value (for parameters, see legend to Fig. 7). It is possible, therefore, that negative cooperativity between the third and fourth Ca^{2+} ions binding to the closed conformation, which is not present in the open conformation, accounts for the position of the *mslo* G-V relation at [Ca] $> \sim$100 μM.

Another means by which we might relax the MWC constraint that the binding sites are acting independently is to suppose that in either the closed or open conformations of the channel the affinity of a given Ca^{2+} binding site changes depending on whether the binding sites on one or two adjacent subunits are already occupied. Scheme III in Fig. 3 *B* represents this idea. In this scheme, each tier is formally equivalent to a square version of the well known KNF model of allosteric interactions between subunits (Koshland et al., 1966). These types of interactions were also considered by Pauling (1935). Because under this idea there is a difference in free energy between a channel with two adjacent sites occupied and one with two diagonally opposed sites occupied, an additional state in each tier is necessary. Once the dissociation constants for a site with zero (K_{XA}) or one (K_{XB}) neighbor occupied are defined, the dissociation constant for a site with two neighbors occupied is determined ($K_{XC} = K_{XB}^2/K_{XA}$). Two free parameters therefore determine the equilibrium binding of Ca^{2+} to each tier of the model. Shown in Fig. 7 *C* is a fit of scheme III to the same data as shown in Fig. 7, *A* and *B*. The dissociation constants for this fit are K_{CA} = 0.046 μM, K_{CB} = 1.42 μM, K_{CC} = 43.90 μM, K_{OA} = 0.047 μM, K_{OB} = 0.100 μM, K_{OC} = 0.213 μM. In general, two-tiered KNF models provide some improvement over voltage-dependent MWC models in fitting the *mslo* data at [Ca] above 124 μM ($P <$ 0.01 for all patches). These models, however, do not fit as well as general 10-state models ($P < 0.01$ for all patches), and the small dissociation constants often associated with the best fit (K_{CA} and K_{OA} above) make it difficult to fit the kinetic data (see below).

An alternative explanation for shifts in G-V curve position at very high [Ca] comes from the work of Wei et al. (1994) (see also Solaro et al., 1995). In their experiments they found that when 10 mM Mg^{2+} was present in the internal solution no further shifting of the *mslo* G-V relation was observed with [Ca] above 100 μM. They suggested that there is a second divalent cation binding site(s) on the *mslo* channel that is less specific for Ca^{2+} over Mg^{2+} than what might be considered the primary site(s), and that at high [Ca] it is Ca^{2+} binding to this second site, perhaps screening a surface charge, that is responsible for the leftward G-V curve shifts above $\sim$100 μM [Ca]. Under this hypothesis, 10 mM Mg^{2+} in the internal solution saturates this site and no further effects of high [Ca] are expected. Clearly, more investigation into this phenomenon will be important. When the G-V data from [Ca] above 124 μM were excluded from the fitting, each of the models discussed in relation to Fig. 7 performed similarly, with somewhat better fits produced as the number of free parameters increased.[3]

P_{open} as a Function of [Ca]

The steady state behavior of *mslo* and model channels can also be compared by looking at P_{open} as a function of [Ca]. In Fig. 8, the data of Fig. 5 *A* are shown converted to Ca^{2+} dose-response form (*filled circles*). Simulated voltage-dependent MWC model data are included as well (*open circles*). Each curve represents a different voltage. Both real data and simulated model points were fitted (*solid curves*) with the Hill equation (Hill, 1910):

$$G/G_{max} = \left[A \frac{1}{1 + \left(\frac{K_D}{[Ca]} \right)^n} \right] \quad (8)$$

The parameters for these fits are plotted in Fig. 8, *C–E*. As over this [Ca] range there is a fairly good agreement between the model and the data in Fig. 5 *A*, it is not surprising that viewed in this way the real and simulated data appear similar (Fig. 8, *A* and *B*). Fitting these data with the Hill equation, however, serves to illustrate some important characteristics shared by *mslo* and voltage-dependent MWC models. Both real data and simulated voltage-dependent MWC model behavior suggest that the maximum extent of channel activation decreases at negative potentials (Fig. 8 *C*). Both systems produce Hill coefficients between 1.5 and 2.0 over a broad range of voltages (Fig. 8 *D*); however, *mslo* Hill coefficients closer to 3 are often observed at voltages greater than +50 mV.[4] This is because the *mslo* dose-response curves are slightly more sigmoid than the

[3]For each patch, the two-tiered KNF scheme fit significantly better than the voltage-dependent MWC scheme ($P < 0.01$), and the general 10-state scheme fit significantly better than the two-tiered KNF scheme ($P < 0.05$).

[4]Models of the form of scheme II actually do not predict a change in Hill coefficient as a function of voltage. The change in model Hill coefficient with voltage in Fig. 8 *D* is due to a voltage-dependent shift in the region of the dose–response curve emphasized in the fitting. The true Hill coefficient, defined as the maximum slope of a plot of log ($P_{open}/(P_{open-max} - P_{open})$) vs. log([Ca]), is a complicated function of [Ca] and all the Ca^{2+} dissociation constants in the model. It can be found by setting the second derivative of the function representing log ($P_{open}/(P_{open-max} - P_{open})$) with respect to log([Ca]) equal to 0, solving for [Ca], and substituting this value of [Ca] into the expression for the first derivative with respect to log([Ca]). For the model in Fig. 8, this value is 2.10. As is well known, however, the model's Hill coefficient would change with L, and therefore voltage, if the fraction of binding sites occupied by Ca^{2+} is measured instead of P_{open} (Wyman and Gill, 1990).

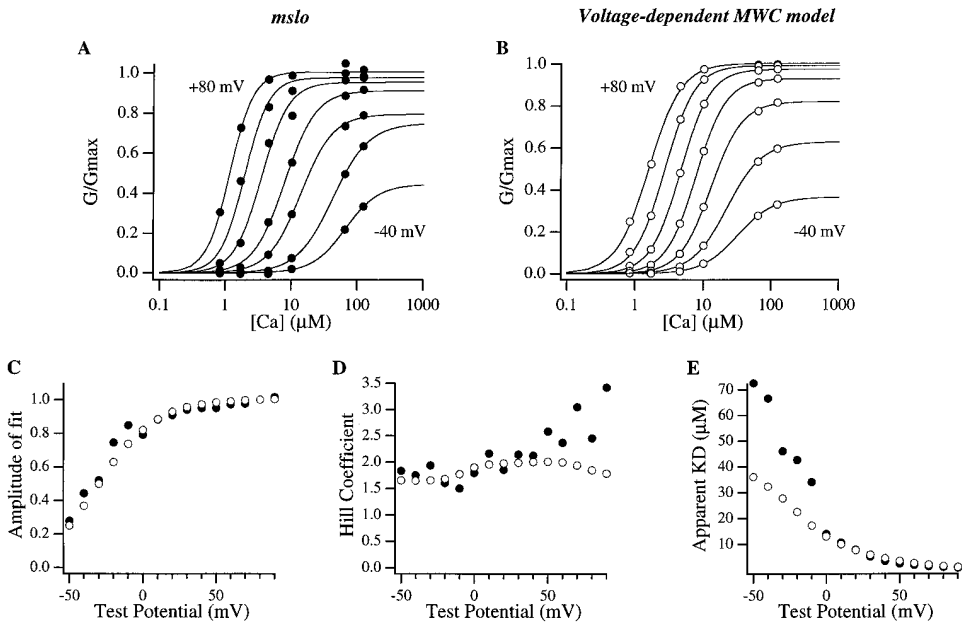

FIGURE 8. *mslo* (*A*) and voltage-dependent MWC model (*B*) Ca^{2+} dose-response curves are plotted for seven different voltages ranging from −40 to +80 mV in 20-mV steps (*symbols*). Each curve in *A* and *B* has been fitted with the Hill equation (Eq. 8) (*solid curves*) and the parameters of these fits are plotted as a function of voltage in *C, D* (see footnote 4), and *E. mslo* data and fit parameters are indicated with (●). Simulated data and fit parameters are indicated with (○). Data are from patch 1 (Fig. 5 *A*). The voltage-dependent MWC model parameters used for these simulations are those listed in Table III. Similar data from patch 1 were displayed in Cui et al. (1997) (Fig. 13).

model curves at these potentials (Fig. 8, *A* and *B*). Both systems also demonstrate an increase in the apparent affinity of the channel for Ca^{2+} as voltage is increased (Fig. 8 *E*) (Barrett et al., 1982; Moczydlowski and Latorre, 1983; Markwardt and Isenberg, 1992; Cui et al., 1997). This might appear to suggest that Ca^{2+} binding steps are voltage dependent (Moczydlowski and Latorre, 1983; Markwardt and Isenberg, 1992). However, voltage-dependent MWC models predict this behavior without supposing voltage dependence in Ca^{2+} binding steps. This is because in the model both Ca^{2+} and voltage alter the free energy difference between closed and open. As the voltage is increased, more energy is contributed to the central equilibrium by the electric field, and, therefore, fewer Ca^{2+} must bind to the channel to bring it to a given P_{open}. This is illustrated in Fig. 6 *E* where open probability is plotted as a function of the mean number of Ca^{2+} ions bound to the model channel at several voltages.

Kinetic Behavior

A more demanding test of any gating model is to mimic the nonstationary gating behavior of the protein being studied. As described below, we attempted to fit *mslo* macroscopic current kinetics with voltage-dependent MWC models. To do so we had to reconcile the fact that, but for a brief delay in the onset of activation, both *mslo* current activation and deactivation can be described by an exponential function over a wide range of [Ca] and membrane voltages (Cui et al., 1997), yet the solution of a 10-state Markov system has nine exponential components. Some of these components may be relatively small in amplitude, and some may have similar time constants. The challenge then is to find conditions under which scheme II behaves like an apparently more simple gating system.

It seems reasonable to suppose that the time course of current relaxation reflects, in part, the vertical rate of flux between open and closed, and, in part, the time it takes for the channels to redistribute horizontally as the net motion between closed and open draws channels away from one tier and to the other. It might be, therefore, that if one of these processes was considerably slower than the other, the kinetics of the system would be dominated by the slower process. In fact, for models of the form of scheme II it is possible to show that in the limit that the equilibration of Ca^{2+} binding steps becomes very fast relative to the vertical transition rates such that each horizontal elementary step can be considered to be at equilibrium at all times, the kinetics of scheme II become monoexponential (see Eigen, 1967; Wu and Hammes, 1973). The time-dependent solution for scheme II in this limit becomes

$$P_{open}(t) = \left[\frac{\alpha}{\alpha+\beta}\right]_{\infty} - \left(\left[\frac{\alpha}{\alpha+\beta}\right]_{\infty} - \left[\frac{\alpha}{\alpha+\beta}\right]_{0}\right)e^{-(\alpha+\beta)t} \quad (9a)$$

$$\alpha = (\alpha_0 f_{C0} + \alpha_1 f_{C1} + \alpha_2 f_{C2} + \alpha_3 f_{C3} + \alpha_4 f_{C4}) \quad (9b)$$

$$\beta = (\beta_0 f_{O0} + \beta_1 f_{O1} + \beta_2 f_{O2} + \beta_3 f_{O3} + \beta_4 f_{O4}) \quad (9c)$$

where α_X and β_X represent closed-to-open and open-to-closed vertical rates constants, respectively, and f_{CX} and f_{OX} represent the fraction of closed (f_{CX}) or open (f_{OX}) channels occupying state x at a given [Ca]. The macroscopic time constant given by $(1/\alpha + \beta)$ is determined by an average of all the vertical rate constants in the scheme, weighted by the fraction of closed (for αs) or

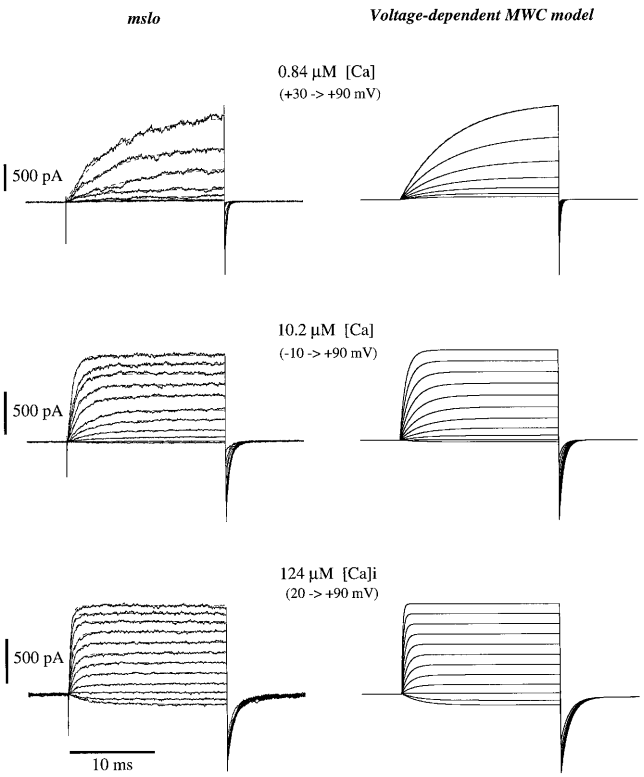

FIGURE 9. *mslo* (*left*) and voltage-dependent MWC model (*right*) traces determined at the indicated [Ca] and membrane voltages. Voltage steps were 20-ms long from the following holding voltages: 0 (0.84 μM [Ca]), −100 (10.2 μM [Ca]), and −120 mV (124 μM [Ca]). In each current family, the voltage increment was 10 mV. Repolarizations were to −80 mV. For display, model and *mslo* current families were scaled to have the same maximum amplitude at +90 mV. Single exponential fits to the activation time courses are superimposed on both the *mslo* and model traces. The fits to the model traces are hard to discern as they follow closely the time courses of activation. Data and model are from patch 1 (see Table III).

open (for βs) channels that precede each vertical transition. The simple kinetic behavior of *mslo* suggests something approximating this situation is occurring. If, on the other hand, we suppose that voltage-dependent transitions are very rapid relative to Ca^{2+} binding transitions, the kinetics of scheme II do not converge to monoexponential behavior as is observed in the data (Cui et al., 1997, and Fig. 9), but rather, each population of channels with a given number of Ca^{2+} bound would appear to gate independently, producing five exponential components in the macroscopic current kinetics.

The kinetics of *mslo* macroscopic currents were fitted to voltage-dependent MWC models using the following procedure. The on rates for Ca^{2+} binding to each subunit were assumed to be at least as fast as is reasonable (10^9 $M^{-1}s^{-1}$) given the diffusion limit for Ca^{2+} binding and the on rates reported for other Ca^{2+} binding proteins (Falke et al., 1994; Cui et al., 1997). Interactions between Ca^{2+} and surface charge could make the Ca^{2+} binding rates even faster. The Ca^{2+} off rates were then constrained by the dissociation constants determined from fitting the steady state data. Likewise, for each vertical step in the model one rate constant was free to vary, while the other was then constrained by the steady state fit. No other constraints were placed on the vertical rate constants except that closed-to-open rate constants were made to increase as the number of bound Ca^{2+} increased. The total gating charge associated with the central conformational change was determined by the steady state fit while the proportion of charge moving in forward and backward transitions was allowed to vary within this constraint. To obtain reasonable fits to the kinetic data, we found that the total gating charge had to be less than that which produced the best fits to the steady state data, this then required smaller $L(0)$ values as well. Good fits to the steady state data, however, were found with these parameters (Fig. 5, *dashed lines*). The parameters used to model both *mslo* steady state and kinetic behavior are listed in Table III.

Shown in Fig. 9 (*left*) are current families recorded from the patch of Fig. 5 *A* at 0.84, 10.2, and 124 μM [Ca]. On the right are traces generated from the voltage-dependent MWC model for this patch (Table III). Each model trace was multiplied by a common factor that made the amplitude of the model current at +90 mV equal to that of the data. Because under the conditions employed, and over this voltage range, the *mslo* single channel i-V relation is linear (Butler et al., 1993; Cox et al., 1997), this normalization procedure is valid. Clearly, there is a qualitative similarity between the data and the model both in terms of kinetics and current amplitude. The parameters for this fit are listed in Table III (Patch 1). Similar fits were obtained with voltage-dependent MWC models for the two other patches (Table III). In each case, model activation kinetics were well described by a single exponential function. In Fig. 9, single exponential fits to the time courses of activation are superimposed on both model and *mslo* currents; however, the fits to the model currents are hard to discern as they follow very nearly the activation time course.

To compare better the kinetics of voltage-dependent MWC models to those of *mslo*, data and model currents were superimposed and scaled to have the same amplitudes (Figs. 10 and 11). At high final open probabilities, the data and model currents activate more rapidly as the voltage is made more positive or [Ca] is increased (Figs. 9 and 10). As understood through the model, the effect of voltage is due to an increase in the magnitude of all the closed-to-open rate constants as the voltage is made more positive. At high open probabilities, these rate constants are largely responsible for the overall kinetic behavior. The acceleration of the activation time

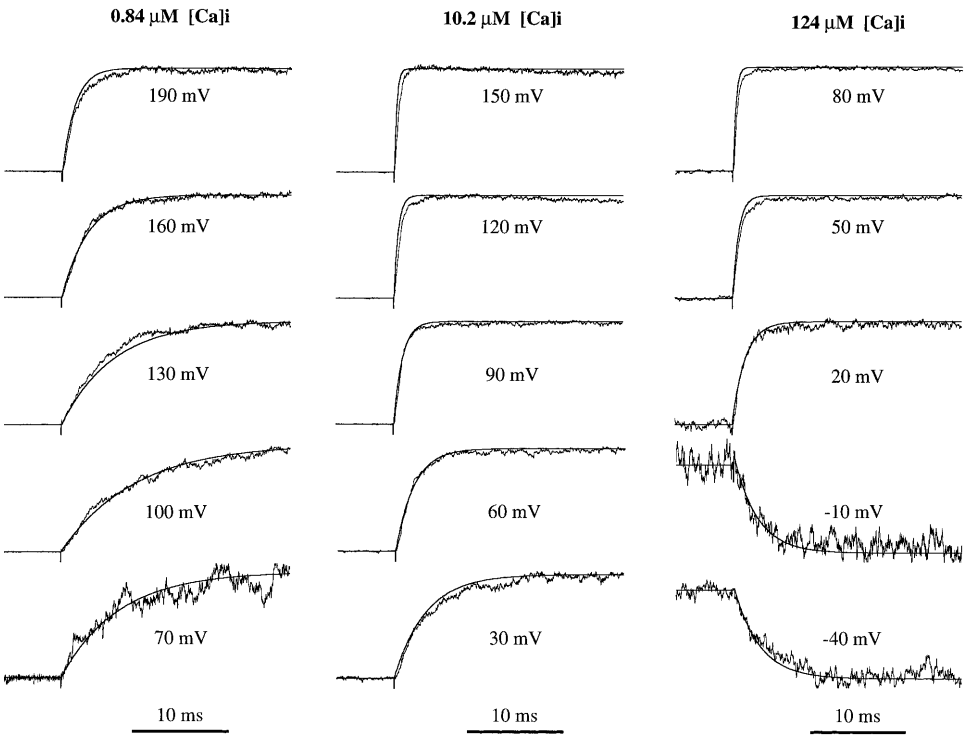

FIGURE 10. Comparison of *mslo* and voltage-dependent MWC model macroscopic activation kinetics. *mslo* and model traces are shown normalized to their maximum values and superimposed. [Ca] and membrane voltages are as indicated. Holding voltages for each [Ca] are as stated in the legend to Fig. 9. Data and model are from patch 1 (see Table III).

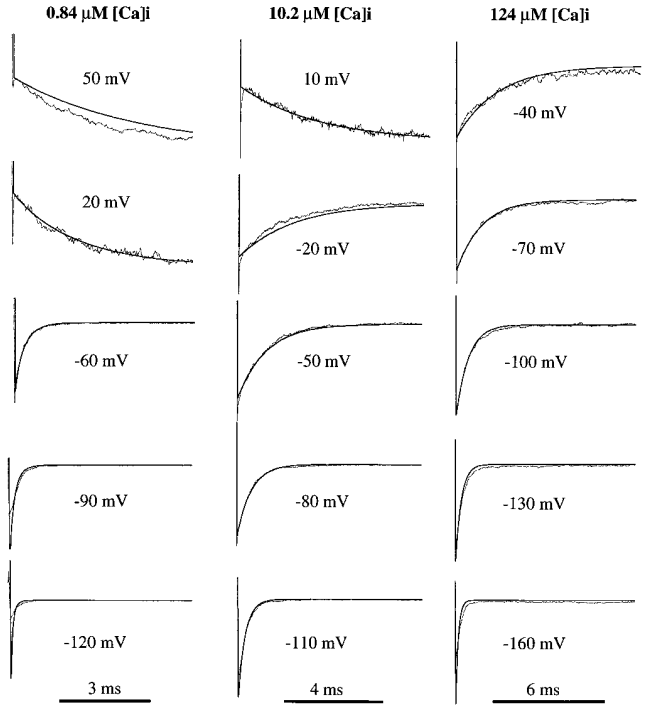

FIGURE 11. Comparison of *mslo* and voltage-dependent MWC model macroscopic deactivation kinetics. *mslo* and model currents are shown normalized to their values 200 μs after stepping to the indicated voltage from a voltage at which the channels were near maximally activated, and superimposed. Prepulse voltages were +180 (0.84 μM [Ca]), +100 (10.2 μM [Ca]), and +90 mV (124 μM [Ca]). [Ca] are as indicated. Data and model are from patch 1 (see Table III).

course by [Ca] also can be understood through the model. Considering Eq. 9, as more Ca^{2+} ions bind to the channel, the fast closed-to-open rate constants on the right hand side of the model become more heavily weighted than the slower closed-to-open rate constants on the left. Faster macroscopic activation kinetics result. Deactivation of model currents to low final open probabilities is dominated by the open-to-closed rates constants. Depolarization decreases the magnitude of these rate constants and slows deactivation (Fig. 11). Increases in [Ca] also slow deactivation because as [Ca] is increased, more weight is given to the slower open-to-closed rate constants on the right hand side of the model than to the faster open-to-closed rate constants on the left.

While the time courses of *mslo* and voltage-dependent MWC model currents are often similar, there is a clear tendency for the model currents to be faster than the data when current relaxations are very rapid (at highly positive voltages and high [Ca] for activation, and highly negative voltages and low [Ca] for deactivation). Also, at negative potentials and low [Ca], the time course of model deactivation deviates from exponential behavior. This is because under these conditions, the open-to-closed transitions do not equilibrate slowly enough relative to the Ca^{2+} binding equilibria so as to allow the Ca^{2+} binding equilibria to always be very close to steady state. In Fig. 11, for example, the model current in the lower left panel (0.84 μM [Ca]; −120 mV)

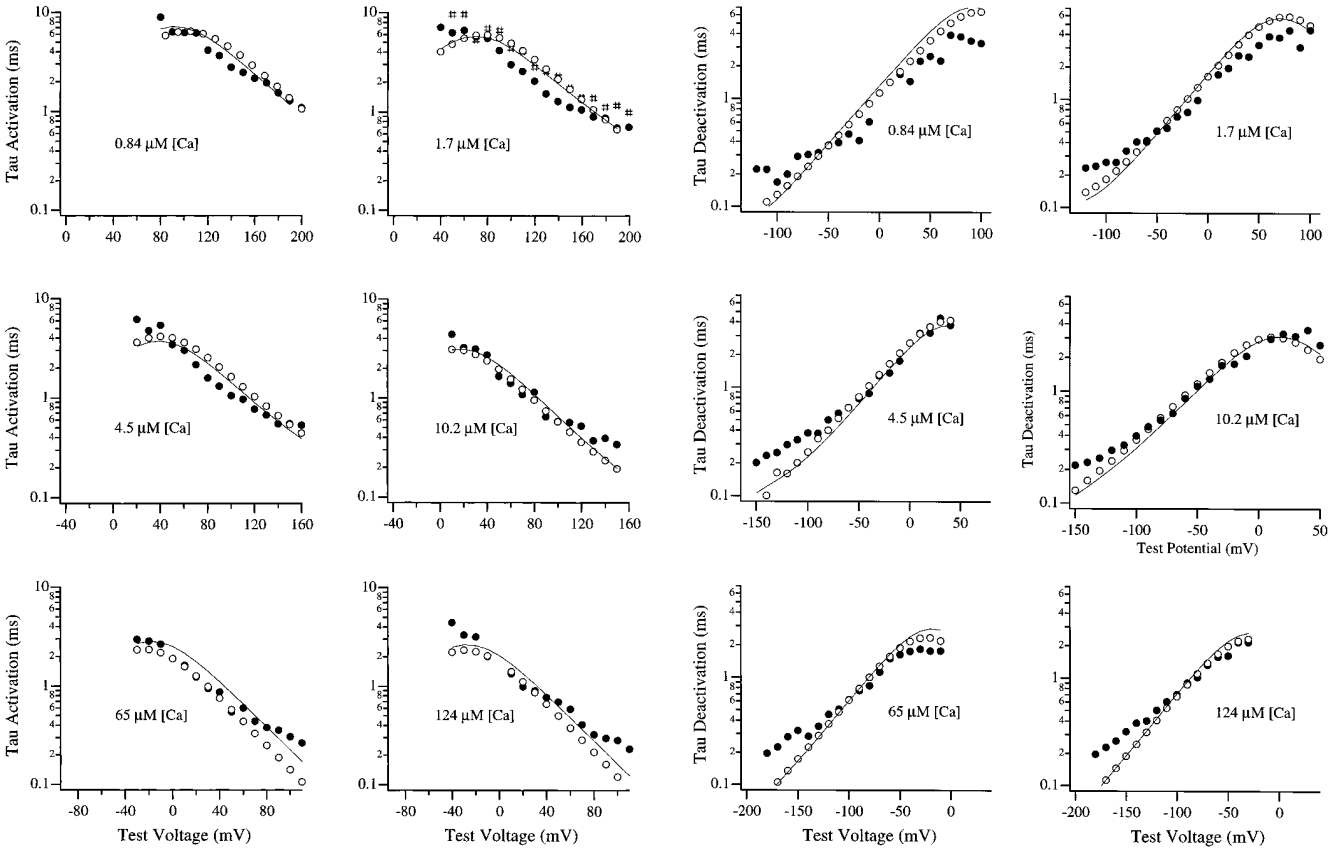

FIGURE 12. Comparison of *mslo* and model macroscopic activation kinetics over a wide range of conditions. [Ca] are as indicated. *mslo* (●), voltage-dependent MWC model (○), and general 10-state model (*solid lines*) traces were fitted with exponential functions starting 200 μs after the beginning of a voltage step to the indicated test voltage. The time constants of these fits are plotted as a function of test voltage. Two sets of data are displayed for 1.7 μM [Ca], corresponding to data recorded at the beginning (●) and the end (#) of the experiment. Notice the change in range of the voltage axis as [Ca] is increased. Holding voltages were: −50 (0.84 μM [Ca]), −80 (1.7 μM [Ca]), −100 (4.5 μM [Ca]), −100 (10.2 μM [Ca]), −120 (65 μM [Ca]), and −120 mV (124 μM [Ca]). Data are from patch 1. The voltage-dependent MWC model parameters are given in Table III. The general 10-state model parameters are as follows: $L(0) = 1{,}647$, $Q = 1.40e$, $K_{C1} = 10.08$ μM, $K_{C2} = 5.22$ μM, $K_{C3} = 5.82$ μM, $K_{C4} = 70.64$ μM, $K_{O1} = 0.890$ μM, $K_{O2} = 0.764$ μM, $K_{O3} = 0.862$ μM, $K_{O4} = 1.52$ μM, $C_0 \rightarrow O_0 = 2.75$ s^{-1}, $C_1 \rightarrow O_1 = 6.0$ s^{-1}, $C_2 \rightarrow O_2 = 32$ s^{-1}, $C_3 \rightarrow O_3 = 165$ s^{-1}, $C_4 \rightarrow O_4 = 1{,}000$ s^{-1}, $O_0 \rightarrow C_0 = 4{,}529.2$ s^{-1}, $O_1 \rightarrow C_1 = 872.7$ s^{-1}, $O_2 \rightarrow C_2 = 681.5$ s^{-1}, $O_3 \rightarrow C_3 = 520.1$ s^{-1}, $O_4 \rightarrow C_4 = 67.6$ s^{-1}, qforward = $0.70e$, qbackward = $-0.70e$.

FIGURE 13. Comparison of *mslo* and model macroscopic deactivation kinetics over a wide range of conditions. [Ca] are as indicated. *mslo* (●), voltage-dependent MWC model (○), and general 10-state model (*solid lines*) currents were fitted with exponential functions starting 200 μs after the beginning of a voltage step to the indicated test voltage from a depolarized voltage where the channels were near maximally activated. The time constants of these fits are plotted as a function of test voltage. Prepulse potentials were: +180 (0.84 μM [Ca]), +160 (1.7 μM [Ca]), +120 (4.5 μM [Ca]), +100 (10.2 μM [Ca]), +90 (65 μM [Ca]), and +90 mV (124 μM [Ca]). Notice the change in range of the voltage axis as [Ca] is increased. Data are from patch 1. The voltage-dependent MWC model parameters are given in Table III. The general 10-state model parameters are given in Fig. 12.

is better fit by a double rather than a single exponential. The fast component of this fit has a time constant of 34 μs. No such fast component is evident in the data. However, in our experiments such a fast component, if present, would have been difficult to distinguish from the capacity transient, and would have been blunted by the analogue filter employed (four pole low pass bessel, 10 kHz).

To compare *mslo* and model macroscopic kinetics over a wider range of conditions, the relaxation time courses of both model and *mslo* currents were fitted with single exponential functions, and the time constants of these fits are plotted as a function of voltage for six different [Ca] in Figs. 12 (activation) and 13 (deactivation). The major effect of an increase in [Ca] is to shift both activation and deactivation τ-V curves leftward along the voltage axis (DiChiara and Reinhart, 1995; Cui et al., 1997) (notice the changes in the range of the voltage axis in Figs. 12 and 13). As was evident in Figs. 10 and 11, when relaxation is very rapid, the model traces (time constants represented by open circles, Figs. 12 and 13) often relax more quickly than the data

(time constants represented by filled circles, Figs. 12 and 13). There appears to be something limiting the kinetic behavior of the *mslo* channel that is not accounted for by the model. Also, the slowest activation time constants are usually slower in the *mslo* data than predicted by the model. Overall, however, voltage-dependent MWC models do a fairly good job at mimicking the shifting nature of the *mslo* τ-V curves as [Ca] is varied.

To examine whether the discrepancies between the shapes of the *mslo* and voltage-dependent MWC model τ-V curves are due to the restrictions placed on the Ca^{2+} dissociation constants by the MWC assumption that the Ca^{2+} binding sites act independently, the kinetic data from patch 1 was fitted with a general form of scheme II. The results of this fit are shown as solid curves on the graphs in Figs. 12 and 13. The general 10-state model behaves very much like the voltage-dependent MWC model. This result suggests that it is not the assumption of binding site independence that leads to the discrepancies between the kinetic data and voltage-dependent MWC models, but, more likely, the assumption that the channel's voltage sensors move in a completely concerted manner may need to be relaxed.

DISCUSSION

We have approached the modeling of BK channel gating by first considering the most general system of states that is required to conform to what is known, or likely to be true, about the structure of these channels, and then simplifying this system of states to a manageable number using adaptations of widely used models for allosteric conformational changes. From the simple premise that each subunit can bind one Ca^{2+} molecule and undergo one voltage-dependent conformational change arises 55 physically distinct states that must exist and therefore contribute to the kinetic behavior of the channel. This large number of states is beyond what can be dealt with analytically under non–steady state conditions, and larger than Markov models typically used to describe the gating of ion channels. The complexity arises here because BK channels respond to two stimuli, Ca^{2+} and membrane voltage, and we have chosen to model the effects of changes in these stimuli simultaneously. In such circumstances, very simple physical pictures lead to many allowable protein conformations. The fact that *slo* α subunits expressed alone form homomultimeric channels helps to reduce the number of distinct channel conformations. Even a homotetrameric *slo* channel, however, could have a conformational space comprised of many more than 55 states. For example, if each subunit could undergo two sequential voltage-dependent steps instead of one, as has been proposed for the *shaker* K^+ channel, even without making distinctions based on subunit position, 126 distinct conformations of the protein would result. This is without considering conformational changes occurring at or below the time resolution of electrophysiological measurements. In the case of *mslo*, however, two observations suggest that voltage-dependent gating steps are highly concerted and therefore might be modeled as a single conformational change without losing a great deal of ability to mimic channel gating. The first is that macroscopic current kinetics are often well approximated by a single exponential function over a wide range of conditions (Cui et al., 1997), suggesting a single rate limiting step between closed and open. The second is that the *mslo* steady state G-V relation can be approximated by a simple Boltzmann function at many [Ca] (Butler et al., 1993; Wei et al., 1994; Cui et al., 1997). While the data do not exactly conform to these functions (as will be discussed below), the degree to which they do conform suggests a concerted series of steps between closed and open. Combining the movement of the channel's four hypothetical voltage sensors into a single step leads to models of the form of scheme II.

The simplest form of scheme II occurs when each Ca^{2+} binding site is independent in both the closed and open conformations, and the opening of the channel changes the affinity of all Ca^{2+} binding sites equivalently. In this case, scheme II becomes a voltage-dependent version of the well known MWC model of allosteric proteins (Monod et al., 1965). MWC models have been used to model the conformational equilibria of many of the best studied allosteric proteins (see Perutz, 1976; Neet, 1995). This prompted us to examine their ability to mimic *mslo* gating. As discussed above, several discrepancies between *mslo* gating and the behavior of voltage-dependent MWC models were discovered: (*a*) the models fail to predict the position of the *mslo* G-V relation at very high [Ca], (*b*) under conditions in which relaxations are very rapid, model traces often relaxed more rapidly than the data, (*c*) the slowest activation time constants at a given [Ca] are usually slower in the data than predicted by the model, (*d*) any changes in the maximum slope of the *mslo* G-V relation as a function of [Ca] are not accounted for by the models, and (*e*) at low [Ca] and negative potentials, the models predict a fast component of deactivation that is not clearly evident in the data. These discrepancies are certainly important, and are very likely pointing towards a better understanding of the gating of BK channels than can be gained from models of this form. Relaxing the constraint that the binding sites act independently did to some extent ameliorate the difficulty in fitting the *mslo* G-V relations at high [Ca]; however, it did not improve the kinetic fits.

On the other hand many aspects of *mslo* gating can be understood through voltage-dependent MWC models: (*a*) monoexponential relaxation kinetics over a

wide range of conditions (Cui et al., 1997), (*b*) Boltzmann-like G-V relations, (*c*) macroscopic activation rate constants that increase with voltage and increase with [Ca] to saturation (DiChiara and Reinhart, 1995; Cui et al., 1997), (*d*) macroscopic deactivation rate constants that decrease with voltage and decrease with [Ca] to saturation (DiChiara and Reinhart, 1995; Cui et al., 1997), (*e*) the apparent Ca^{2+} affinity of the channel, as judged by the channel's steady state open probability, is strongly voltage dependent, while the apparent affinity, as judged by saturation of the activation kinetics, is less so (Cui et al., 1997), (*f*) at most potentials, it takes less Ca^{2+} to saturate the steady state conductance than it does to saturate the macroscopic rate constant of activation (Cui et al., 1997), (*g*) the channel can be very nearly maximally activated by voltage without binding Ca^{2+} (Cui et al., 1997), (*h*) plots of steady state conductance vs. [Ca] are often best fit with Hill coefficients close to 2 (Barrett et al., 1982; Methfessel and Boheim, 1982; Golowasch et al., 1986; Cornejo et al., 1987; Oberhauser et al., 1988; Sheppard et al., 1988; MacKinnon and Miller, 1989; Reinhart et al., 1989; Tabcharani and Misler, 1989; Segal and Reuss, 1990; Markwardt and Isenberg, 1992; Perez et al., 1994; DiChiara and Reinhart, 1995), and (*i*) a nonlinear $V_{1/2}$ vs. log[Ca] plot (Wei and Salkoff, 1986; DiChiara and Reinhart, 1995; Cui et al., 1997). In many respects, voltage-dependent MWC models appear to provide a reasonable general description of the channel's gating behavior and are useful in understanding the molecular mechanisms of *mslo* gating.

The dose-response relationships of many allosteric proteins have been modeled using the MWC formalism, and putative T and R states of several of these proteins have been crystallized. A list of these proteins includes hemoglobin, aspartate transcarbamoylase, phosphofructokinase, glycogen phosphorylase, fructose bisphosphatase, pyruvate kinase, and others (for reviews see Perutz, 1989; Dittrich, 1992; Neet, 1995). The allosteric behavior of some ion channels have also been modeled in this way (Marks and Jones, 1992; Goulding et al., 1994; Tibbs et al., 1995; Edelstein et al., 1996; Galzi et al., 1996; Varnum and Zagotta, 1996). Of these, the cyclic nucleotide–gated (CNG) channels of retina and olfactory epithelium are most similar to *mslo*. These channels are thought to be tetramers with a single cyclic nucleotide binding site in each monomer (Liu et al., 1996). Like *mslo*, their amino acid sequences suggest they are structurally similar to voltage-gated ion channels with a specialized domain attached to facilitate ligand binding (Kaupp et al., 1989). Also like *mslo*, channel opening has been demonstrated in the absence of bound ligand (Tibbs et al., 1995), subunits appear to change conformation in a concerted manner as the channel opens (Varnum and Zagotta, 1996), and the cyclic nucleotide dose-response relations of CNG channels can be fitted with MWC models (Goulding et al., 1994; Varnum and Zagotta, 1996) (for a review of cyclic nucleotide–gated channel properties see Zagotta and Siegelbaum, 1996). These similarities suggest a common mechanism by which ligand binding is coupled to channel opening. Studies of either channel type may therefore contribute to the understanding of the other.

Unlike CNG channels, however, BK channels are significantly voltage dependent. The equilibrium gating of BK channels can therefore be examined under a wider range of conditions than has been possible for CNG channels. Determining the open probability of *mslo* as a function of [Ca] at 10-mV increments spanning a 100-mV range (the experiment of Fig. 8) is in many respects similar to measuring the substrate activation curve of a classic allosteric protein at many effector concentrations. The main differences between these experiments being that with channels we are in the unusual position of being better able to measure the fraction of channels in the open conformation than the number of ligands bound to the channel, and voltage, unlike an effector, can influence equilibria in either direction. Experiments involving both substrate and effector have contributed greatly to the functional understanding of many allosteric enzymes (for reviews see Perutz, 1989; Neet, 1995). The ability to manipulate *mslo* gating with both Ca^{2+} and voltage therefore holds promise for a more detailed understanding of the gating of these proteins in the future. Also promising, with voltage perturbations, the nonstationary kinetic behavior of *slo* channels can be examined in detail both with macroscopic currents, as was done here, and at the single channel level. These types of data, however, put greater demands on models of *mslo* gating than, for example, the models used to describe the gating of CNG channels. The degree to which voltage-dependent MWC models fail to mimic the gating of *mslo* therefore may not indicate that these models are less valid for *mslo* than other allosteric proteins, but rather in some instances the demands put on the models by the *mslo* data are greater.

Often, careful examination of allosteric systems initially characterized as MWC systems reveals inconsistences with this simple model. For example, two main conformations of hemoglobin (R and T) have been crystallized (Perutz, 1976). However, experiments using the irreversible ligand Fe(III)-CN have revealed that once a ligand is bound to one subunit of an $\alpha\beta$ dimer, the protein is much more likely to convert to its R conformation if the next ligand binds to a subunit of the other $\alpha\beta$ dimer rather than to the same dimer (Holt and Ackers, 1995). This indicates the presence of intermediate states between the T and R conformations and violates the MWC postulate that binding to any one

site affects all sites equivalently. Experimental evidence also suggests that yeast pyruvate kinase can exist in an intermediate state between T to R (Murcott et al., 1992). The discrepancies between our data and voltage-dependent MWC models are very likely indicating similar complexities. As was shown, models based on the general form of scheme II do at least as well as voltage-dependent MWC models in fitting *mslo* macroscopic current behavior and, in some respects, better. General 10-state models, however, have six more free parameters than do voltage-dependent MWC models, and it was often the case that for these models more than one set of parameters could give reasonable fits to the steady state data. As there are alternative explanations for the leftward shifting of the *mslo* G-V curves at [Ca] over ~100 μM (Wei et al., 1994; Solaro et al., 1995), we are not yet in a position to distinguish between models containing interactions between binding sites in a given conformation and those that do not. In fact, another model we have examined that conforms to scheme II and contains only three free parameters (at equilibrium) can fit the *mslo* data with some success, although not as well as those described. This model is based on the premise that the second Ca^{2+} ion that binds to the channel provides all of the free energy that stabilizes the open conformation relative to the closed. In the sense that a single binding event provides most of the energy stabilizing the open state over the closed, this model is similar to that proposed by McManus and Magleby (1991) to account for the Ca-dependent properties of single skeletal muscle BK channels under steady state conditions. Whether the binding of Ca^{2+} to some sites in the closed or open conformation affects the affinities of the unoccupied sites will be important to determine. However, even without supposing a deviation from strict MWC behavior, both the voltage-dependent MWC models used here and the McManus and Magleby model predict that three Ca^{2+} ions must bind to a channel at +30 mV before it is more likely to be open than closed. Also, with a given number of Ca^{2+} ions bound, they both contain a single step between closed and open.

Already, however, several lines of evidence indicate that more than one voltage-dependent conformational change is necessary for *mslo* channels to move from closed to open, suggesting that better models of *mslo* gating might be constructed if the intermediate states in scheme I were not excluded. First, there is a brief delay in activation of *mslo* macroscopic currents, which can be seen at most [Ca], including very low concentrations where the channels gate without bound Ca^{2+} (Toro et al., 1996; Cui et al., 1997). To account for this delay, multiple steps need to exist between closed and open. Second, gating schemes with a single voltage-dependent conformational change between closed and open predict G-V relations described by a simple Boltzmann function, while better fits to higher powers of a Boltzmann function are indicative of multiple voltage-dependent steps (Sigworth, 1994; Zagotta et al., 1994*a*, 1994*b*). The *mslo* G-V relation often appears fairly well fit by a Boltzmann function, but is usually best fit with a Boltzmann function raised to a power between 1 and 3 (Cui et al., 1997). And third, recent gating current measurements from *slo* channels indicate that gating charge movement precedes channel opening (Horrigan et al., 1996; Ottolia et al., 1996). Models of the form of scheme II predict that ionic and gating current relaxations follow the same time course. In the future, an examination of the properties of models of the form of scheme I may be fruitful as this scheme allows for gating charge movement before channel opening.

Relation to Single Channel Studies

Single channel analysis of both native (McManus and Magleby, 1988, 1991; Art et al., 1995; Giangiacomo et al., 1995; Wu et al., 1995) and cloned (DiChiara and Reinhart, 1995; Lagrutta et al., 1996) BK channels has revealed that these channels exhibit stationary gating kinetics with at least five exponential components to their closed time distribution and at least three exponential components to their open time distribution. How does a system display complex kinetic behavior at the single channel level and relatively simple kinetic behavior when recorded from as a population? What sorts of dwell time distributions do the voltage-dependent MWC models presented here predict? To answer the second question, the Q-matrix methods described by Colquhoun and Hawkes (1981, 1982, 1995*b*) were used to solve for the open and closed time distributions predicted by the voltage-dependent MWC model for patch 1. As might be expected, results of these calculations indicate that under most circumstances the distributions are heavily dominated by a single component whose time constant is well approximated by $1/\alpha$ given by Eq. 9*b* for closed times and $1/\beta$ given by Eq. 9*c* for open times. As discussed above, this is because, under most conditions, model Ca^{2+} binding steps equilibrate rapidly relative to the closed-to-open equilibrium. However, as can be seen in Fig. 14, preliminary results suggest that when comparing model currents to the data, voltage-dependent MWC models appear to mimic the bursting of *mslo*, but fail to reproduce brief closures during the bursts. Several studies indicate that these brief closures contribute significantly to the complexity of the single channel dwell time distributions. When brief (as well as very long) closures are ignored in the analysis, BK channel burst time distributions are dominated by a single component (Methfessel and Boheim, 1982; Magleby and Pallotta, 1983; Moczydlowski and

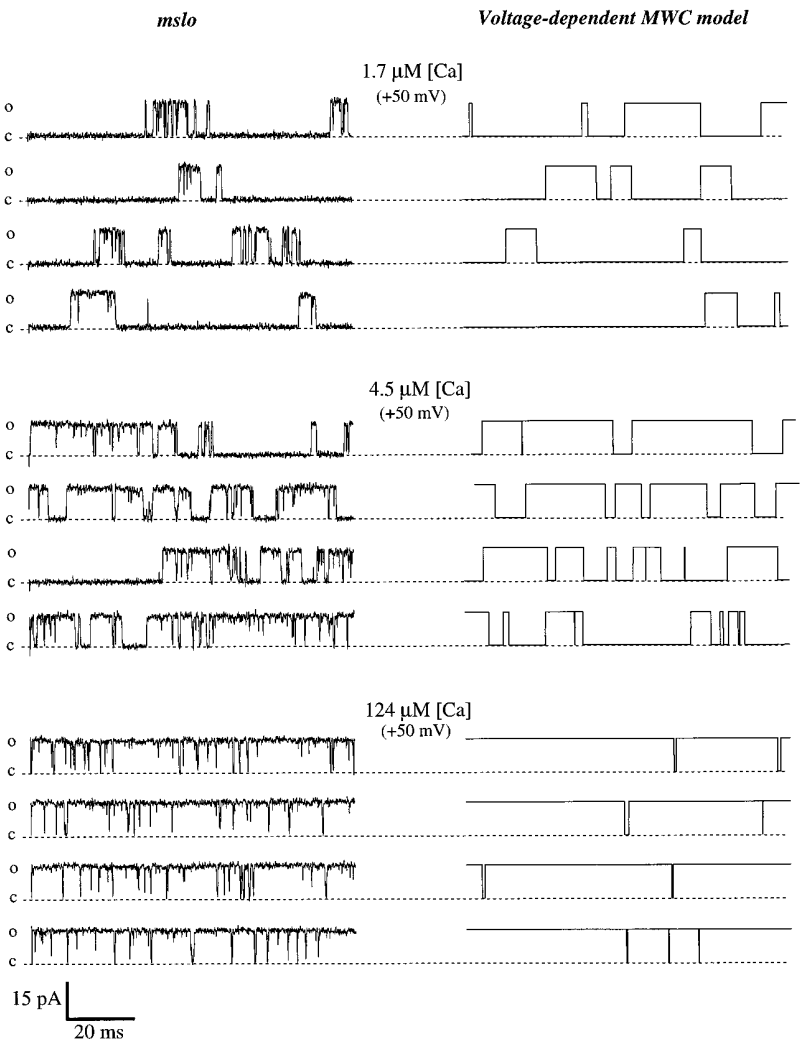

FIGURE 14. Comparison of *mslo* and voltage-dependent MWC model single channel currents. (*Left*) *mslo* data from a single membrane patch. The voltage was held at +50 mV and currents were recorded at the indicated [Ca]. The traces displayed are from consecutive 100-ms time increments. The data were low base filtered at effectively 3.3 kHz before display. (*Right*) Simulated voltage-dependent MWC model single channel currents generated for the same conditions as the data on the left. The model for patch 1 was used. For parameters see Table III.

Latorre, 1983, although a smaller component of bursts comprised of brief single openings is also evident, Magleby and Pallotta, 1983). The question then becomes, how do these brief closures affect the time course of macroscopic BK channel currents? This question has been addressed by Colquhoun and Hawkes (1995*a*) in the context of the following system, which bursts perceptibly when γ is large relative to α and β.

$$C_0 \underset{\beta}{\overset{\alpha}{\rightleftharpoons}} C_1 \underset{\delta}{\overset{\gamma}{\rightleftharpoons}} O_2 \quad 40$$

As pointed out, "when the gaps within bursts are brief, noise and relaxation experiments will give a time constant that corresponds approximately to the mean burst length rather than the mean open time" (Colquhoun and Hawkes, 1995*a*). Some of the complexity of channel gating is not evident in the macroscopic kinetic behavior. Thus, the observation that models designed to mimic macroscopic *mslo* currents do not predict brief closures within bursts is not unexpected. However, this does not excuse the fact that voltage-dependent MWC models fail to predict this feature of BK single channel recordings. What is the origin of these brief closures? One possibility is suggested by scheme I. If in this scheme voltage sensor movement is highly cooperative (as the data suggests), then under most circumstances the final vertical equilibrium preceding each open state will be heavily biased towards opening, creating a situation in which the channel is likely to close briefly to states that precede open, and then reopen producing brief flickers closed such as are observed. The inability of the models of the form of scheme II we have described to account for the complicated single channel kinetics of BK channels may be, therefore, also a consequence of condensing several cooperative voltage-dependent steps into a single step. Another possibility is that brief closures represent sojourns into closed states not involved in the activation pathway (see for example Hoshi et al., 1994). Alterna-

tively, McManus and Magelby (1991) have demonstrated that a subset of scheme II composed of five closed and three open states can account for most of the Ca-dependent stationary gating properties of native skeletal muscle BK channels at +30 mV, including the flickering behavior. This demonstrates that models of the form of scheme II are sufficient to generate such complex single channel kinetics without supposing additional states. However, as they did not study the voltage-dependent properties of these channels, it is not clear how well models like those they proposed could mimic the voltage-dependent kinetics of skeletal muscle BK channel currents. Ultimately, models that can account for both single-channel and macroscopic behavior over a wide range of [Ca] and membrane voltages are desirable. To build such models for *mslo*, a detailed kinetic analysis of single channel gating will be necessary, and the existence of at least as many states as shown in Fig. 2 will need to be taken into account.

Interpretation of Mutant Channel Behavior

Putting aside for the moment the problems with voltage-dependent MWC models, the success of these models in many respects suggests that they may be useful in interpreting modifications or mutations of *slo* channels. A common question, for example, might be: does a particular mutation that alters the apparent affinity of the channel for Ca^{2+} affect the affinity of Ca^{2+} binding or other conformational changes involved in gating? As has become common in the recent literature, changes in channel behavior are often characterized in terms of changes in the relationship between $V_{1/2}$ and log[Ca]. Eq. 6 indicates that changes in $L(0)$, and therefore the intrinsic free energy difference between open and closed, will affect the apparent Ca^{2+} affinity of the model channel, but will not affect the relative spacing of the G-V curves determined at several [Ca]. A plot of $V_{1/2}$ vs. log[Ca], therefore, will not change shape from wild type to mutant. It will simply translate along the voltage axis. This is demonstrated in Fig. 15 *A*, where $V_{1/2}$ vs. log[Ca] is plotted for a hypothetical wild-type voltage-dependent MWC model channel (*asterisks*) and for the case in which $L(0)$ is reduced from 2,000 to 2 (*triangles*). Also shown are the effects of changing other model parameters. For comparison, in Fig. 15 *C*, the curves from Fig. 15 *A* have been shifted so that they have the same $V_{1/2}$ value at 0 [Ca]. Here, the curves corresponding to $L(0) = 2{,}000$ and $L(0) = 2$ superimpose, demonstrating that they have the same shape. This result would suggest that a mutation has not affected the actual affinity of Ca^{2+} binding sites for Ca^{2+}, but rather $L(0)$. On the other hand, according to scheme II, mutations that do affect the shape of the *mslo* $V_{1/2}$ vs. log[Ca] relation could arise in two ways: (*a*) a change in the voltage sensitivity of the channel Q (Fig. 15, *squares*), or (*b*) a change in one or more Ca^{2+} dissociation constants (Fig. 15, *circles*). As can be seen from Eq. 6, a change in Q scales a plot of $V_{1/2}$ vs. log[Ca] by a constant factor, while a change in the affinity of Ca^{2+} binding sites will affect the spacing of the G-V curves in a less predictable manner. One way to distinguish between these possibilities then is to multiply the apparent gating charge of the channel determined from

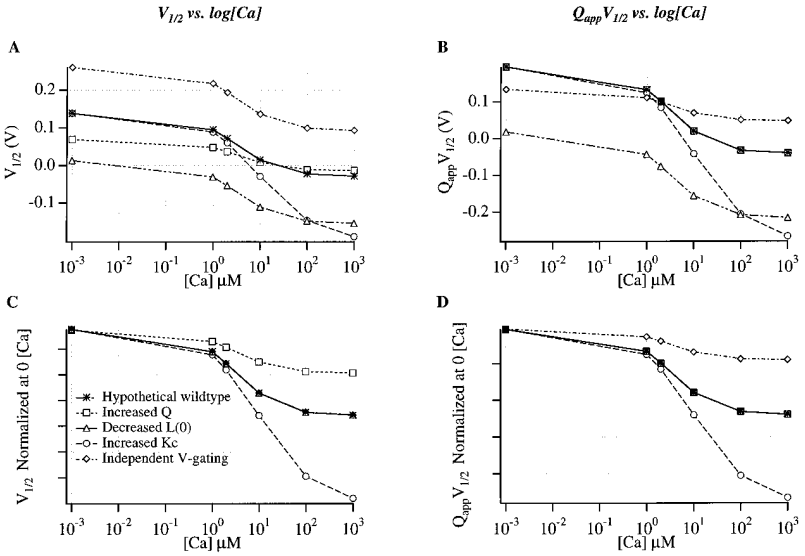

FIGURE 15. The effects of modifications or mutations on model gating behavior. (*A*) Plots of $V_{1/2}$ vs. log[Ca] for a hypothetical wild-type voltage-dependent MWC model channel (●), as well as after four types of modification: an increase in Q to 2.8 (□), a decrease in $L(0)$ to 2 (△), an increase in K_C to 100 μM (○), and elimination of cooperative interactions between voltage-dependent conformational changes (◇). The parameters for the wild-type model are as in Fig. 6 *A*. To simulate a loss of cooperativity between voltage-sensing elements, an expression for the equilibrium open probability of scheme I was used with $L(0) = (1/2{,}000)^{1/4}$, $Q = 0.35$, $K_C = 10$ μM, and $K_O = 1$ μM where these parameters represent the properties of each individual subunit. No cooperativity between Ca^{2+} binding sites or voltage sensing elements was included. (*B*) Plots of $Q_{app}V_{1/2}$ vs. log[Ca] for the same simulated data as in *A*. Q_{app} was determined from Boltzmann fits to the G-V relations for each case. (*C*) The plots in *A* have been shifted so as to have the same $V_{1/2}$ value as the hypothetical wild type at 0 [Ca]. (*D*) The plots in *B* have been shifted so as to have the same $Q_{app}V_{1/2}$ value as the hypothetical wild type at 0 [Ca].

Boltzmann fits by $V_{1/2}$, and then to plot this value vs. log[Ca]. This corrects for changes in the shape of the $V_{1/2}$ vs. log[Ca] relation due to alterations in Q. Plots of $Q_{app}V_{1/2}$ vs. log[Ca] are shown in Fig. 15 *B*. Notice that the wild type and increased Q plots superimpose, while when K_C is altered, the shape of the $Q_{app}V_{1/2}$ vs. log [Ca] plot differs from wild type. This type of plot would therefore be preferable to a plot of $V_{1/2}$ vs. log[Ca] for differentiating changes in Ca^{2+} affinity from changes in the intrinsic energy difference between closed and open.

Another approach to interpreting channel modifications would be to examine the wild type and mutant channel's G-V relation at very low [Ca] where the channel is gating without binding Ca^{2+} (Meera et al., 1996; Cui et al., 1997). Here, according to scheme II, differences in the position of the G-V relation can only reflect changes in $L(0)$ or Q. If it is only Q that has changed, $Q_{app}V_{1/2}$ will be the same for mutant and wild-type channels, while if $L(0)$ has changed, this will not be the case (see Fig. 15 *B*). Of course, if a mutation were to make the shapes of the *mslo* G-V relations at different [Ca] grossly different, this would indicate that interpreting the effects of the mutation in terms of models of the form of scheme II may not be valid.

Since scheme I may more generally represent *mslo* gating behavior than does scheme II, we might ask how modifications or mutations would affect the equilibrium properties of models of the form of scheme I? Restricting the analysis to conditions in which the G-V relations do not change shape as [Ca] is varied, simulations of the behavior of scheme I indicate that, as for scheme II, changes in the voltage-dependent equilibrium constant of each subunit (see Fig. 1 *A*) do not affect the shape of the $V_{1/2}$ vs. log[Ca] curve, only its position along the voltage axis. Likewise, changes in the charge associated with each voltage-dependent step can to a very good approximation be compensated for by multiplying $V_{1/2}$ by the apparent gating charge determined from a simple Boltzmann fit, and then plotting $Q_{app}V_{1/2}$ vs. log[Ca]. For models of the form of scheme I, however, changes in the maximum slope of the G-V curves can also come about through alteration of the cooperative interactions between voltage-dependent steps. A decrease in cooperativity will make the G-V curves more shallow and less well approximated by a Boltzmann function. The spacing of the G-V curves, however, will not be affected by such a modification and, therefore, a plot of $V_{1/2}$ vs. log[Ca] will maintain its shape. This is demonstrated in Fig. 15, *A* and *C*, where the asterisks can be thought of as representing scheme I with highly cooperative voltage-dependent conformational changes, and the diamonds represent scheme I with no cooperativity between voltage sensors. Although a plot of $V_{1/2}$ vs. log[Ca] will maintain its shape after such a mutation, a plot of $Q_{app}V_{1/2}$ vs. log[Ca] will not. It becomes more shallow as cooperativity decreases (Fig. 15, *B* and *D*). Also, unlike changes in Q or K_C, a decrease in voltage sensor cooperativity causes a change in the value of $Q_{app}V_{1/2}$ at 0 [Ca] (Fig. 15 *B*).

Considering the above discussion, according to scheme I, modifications that directly affect Ca^{2+} binding can be distinguished from those affecting gating steps intrinsic to the protein as follows. Given that the G-V curves have a similar shape at each [Ca] after the modification, if plots of both $V_{1/2}$ vs. log[Ca] and $Q_{app}V_{1/2}$ vs. log[Ca] change shape from wild type to mutant, the mutation is likely to be having a direct effect on Ca^{2+} binding constants. Otherwise, it is more likely that the effect is on conformational changes intrinsic to the protein. This is evident in Fig. 15, *C* and *D* where the only relation that differs in shape from wild type in both plots is that for changing K_C.

In conclusion, the work described here demonstrates that many aspects of the gating of a BK channel can be understood through kinetic models that are based on the premise that the channel is a homomultimer with a Ca^{2+} binding site and voltage sensor in each subunit. Of these, voltage-dependent MWC models are the simplest, and yet they can mimic many aspects of *mslo* macroscopic kinetic and steady state behavior. This suggests that the allosteric mechanism of this channel may be similar to those of other allosteric proteins whose behaviors have been modeled with the MWC formalism. To gain a detailed understanding of *mslo* gating, however, more experimentation and more complex models along the lines of scheme I, or even more complex schemes, will be necessary. Very likely, such work will contribute to our understanding of allosteric proteins in general.

We gratefully acknowledge Larry Salkoff for providing the *mslo* clone, and Toshi Hoshi and Dorothy Perkins for developing software used in modeling channel behavior.

This work was supported by a National Institute of Mental Health Silvio Conte Center for Neuroscience Research grant (MH 48108). J. Cui was supported by a postdoctoral fellowship from the Muscular Dystrophy Association. R.W. Aldrich is an investigator with the Howard Hughes Medical Institute.

Original version received 4 April 1997 and accepted version received 11 June 1997.

REFERENCES

Adelman, J.P., K.Z. Shen, M.P. Kavanaugh, R.A. Warren, Y.N. Wu, A. Lagrutta, C.T. Bond, and R.A. North. 1992. Calcium-activated potassium channels expressed from cloned complementary DNAs. *Neuron.* 9:209–216.

Aggarwal, S.K., and R. MacKinnon. 1996. Contribution of the S4 segment to gating charge in the *shaker* K^+ channel. *Neuron.* 16: 1169–1177.

Art, J.J., Y.C. Wu, and R. Fettiplace. 1995. The calcium-activated potassium channels of turtle hair cells. *J. Gen. Physiol.* 105:49–72.

Atkinson, N.S., G.A. Robertson, and B. Ganetzky. 1991. A component of calcium-activated potassium channels encoded by the Drosophila slo locus. *Science (Wash. DC).* 253:551–555.

Barrett, J.N., K.L. Magleby, and B.S. Pallotta. 1982. Properties of single calcium-activated potassium channels in cultured rat muscle. *J. Physiol. (Lond.).* 331:211–230.

Blair, L.A., and V.E. Dionne. 1985. Developmental acquisition of Ca^{2+}-sensitivity by K^+ channels in spinal neurones. *Nature (Lond.).* 315:329–331.

Butler, A., S. Tsunoda, D.P. McCobb, A. Wei, and L. Salkoff. 1993. mSlo, a complex mouse gene encoding "maxi" calcium-activated potassium channels. *Science (Wash. DC).* 261:221–224.

Carl, A., and K.M. Sanders. 1989. Ca^{2+}-activated K channels of canine colonic myocytes. *Am. J. Physiol.* 257:C470–C480.

Colquhoun, D., and A.G. Hawkes. 1981. On the stochastic properties of single ion channels. *Proc. R. Soc. Lond. B Biol. Sci.* 211:205–235.

Colquhoun, D., and A.G. Hawkes. 1982. On the stochastic properties of bursts of single ion channel openings and of clusters of bursts. *Philos. Trans. R. Soc. Lond. B Biol. Sci.* 300:1–59.

Colquhoun, D., and A.G. Hawkes. 1995*a*. The principles of the stochastic interpretation of ion channels. *In* Single Channel Recording. B. Sakmann and E. Neher, editors. Plenum Press, New York. pp. 397–479.

Colquhoun, D., and A.G. Hawkes. 1995*b*. A Q-matrix cookbook: how to write only one program to calculate the single-channel and macroscopic predictions for any kinetic mechanism. *In* Single Channel Recording. B. Sakmann and E. Neher, editors. Plenum Press, New York. pp. 589–633.

Cornejo, M., S.E. Guggino, and W.B. Guggino. 1987. Modification of Ca^{2+}-activated K+ channels in cultured medullary thick ascending limb cells by *N*-bromoacetamide. *J. Membr. Biol.* 99:147–155.

Cox, D.H., J. Cui, and R.W. Aldrich. 1997. Separation of gating properties from permeation and block in *mslo* large conductance Ca-activated K^+ channels. *J. Gen. Physiol.* In press.

Cui, J., D.H. Cox, and R.W. Aldrich. 1997. Intrinsic voltage dependence and Ca^{2+} regulation of *mslo* large conductance Ca-activated K^+ channels. *J. Gen. Physiol.* In press.

DiChiara, T.J., and P.H. Reinhart. 1995. Distinct effects of Ca^{2+} and voltage on the activation and deactivation of cloned Ca^{2+}-activated K^+ channels. *J. Physiol. (Lond.).* 489:403–418.

Dittrich, N. 1992. Regulation of proteins by ligands. *In* Proceedings of The Robert A. Welch Foundation Conferences on Chemical research (Houston: The Robert A. Welch Foundation), pp. 201.

Dworetzky, S.I., C.G. Boissard, R.J. Lum, M.C. McKay, M.D. Post, J.T. Trojnacki, C.P. Chang, and V.K. Gribkoff. 1996. Phenotypic alteration of a human BK (hSlo) channel by hSlobeta subunit coexpression: changes in blocker sensitivity, activation/relaxation and inactivation kinetics, and protein kinase A modulation. *J. Neurosci.* 16:4543–4550.

Edelstein, S.J., O. Schaad, E. Henry, D. Bertrand, and J.P. Changeux. 1996. A kinetic mechanism for nicotinic acetylcholine receptors based on multiple allosteric transitions. *Biol. Cybern.* 75:361–379.

Eigen, M. 1967. Kinetics of reaction control and information transfer in enzymes and nucleic acids. *In* Nobel Symposium. Fast Reactions and Primary Processes in Chemical Kinetics. S. Claesson, editor. Interscience Publishers, New York. pp. 333–369.

Falke, J.J., S.K. Drake, A.L. Hazard, and O.B. Peersen. 1994. Molecular tuning of ion binding to calcium signaling proteins. *Q. Rev. Biophys.* 27:219–290.

Feller, W. 1968. An introduction to probability theory and its applications. 3rd, Volume I. R.A. Bradley, J.S. Hunter, D.G. Kendall, and G.S. Watson, editors. John Wiley and Sons, New York. pp. 509.

Galzi, J.L., S.J. Edelstein, and J. Changeux. 1996. The multiple phenotypes of allosteric receptor mutants. *Proc. Natl. Acad. Sci. USA.* 93:1853–1858.

Giangiacomo, K.M., M. Garciacalvo, H.G. Knaus, T.J. Mullmann, M.L. Garcia, and O. Mcmanus. 1995. Functional reconstitution of the large-conductance, calcium-activated potassium channel purified from bovine aortic smooth muscle. *Biochemistry.* 34: 15849–15862.

Golowasch, J., A. Kirkwood, and C. Miller. 1986. Allosteric effects of Mg2+ on the gating of Ca2+-activated K+ channels from mammalian skeletal muscle. *J. Exp. Biol.* 124:5–13.

Goulding, E.H., G.R. Tibbs, and S.A. Siegelbaum. 1994. Molecular mechanism of cyclic-nucleotide-gated channel activation. *Nature (Lond.).* 372:369–374.

Heginbotham, L., and R. MacKinnon. 1992. The aromatic binding site for tetraethylammonium ion on potassium channels. *Neuron.* 8:483–491.

Hill, A.V. 1910. The possible effects of the aggregation of the molecules of hemoglobin on the dissociation curves. *J. Physiol. (Camb.).* 40:iv–vii.

Holt, J.M., and G.K. Ackers. 1995. The pathway of allosteric control as revealed by hemoglobin intermediate states. *FASEB J.* 9:210–218.

Horn, R. 1987. Statistical methods for model discrimination. Applications to gating kinetics and permeation of the acetylcholine receptor channel. *Biophys. J.* 51:255–263.

Horrigan, F.H., J. Cui, D.H. Cox, and R.W. Aldrich. 1996. Gating charge movement from *mslo* Ca^{2+}-activated K^+ channel measured via admittance analysis. *Biophys. J.* 70:A233.

Hoshi, T., W.N. Zagotta, and R.W. Aldrich. 1994. Shaker potassium channel gating. I: Transitions near the open state. *J. Gen. Physiol.* 103:249–278.

Kaupp, U.B., T. Niidome, T. Tanabe, S. Terada, W. Bonigk, W. Stuhmer, N.J. Cook, K. Kangawa, H. Matsuo, T. Hirose, et al. 1989. Primary structure and functional expression from complementary DNA of the rod photoreceptor cyclic GMP-gated channel. *Nature (Lond.).* 342:762–766.

Koshland, D.J., G. Nemethy, and D. Filmer. 1966. Comparison of experimental binding data and theoretical models in proteins containing subunits. *Biochemistry.* 5:365–385.

Lagrutta, A., J.P. Adelman, and K.L. Magleby. 1996. Wanderlust kinetics and variable Ca^{2+} sensitivity of *dSlo*, a large conductance Ca^{2+}-activated K^+ channel, expressed in oocytes. *Biophys. J.* 70: 2640–2651.

Larsson, H.P., O.S. Baker, D.S. Dhillon, and E.Y. Isacoff. 1996. Transmembrane movement of the *shaker* K^+ channel S4. *Neuron.* 16:387–397.

Latorre, R., C. Vergara, and C. Hidalgo. 1982. Reconstitution in planar lipid bilayers of a Ca^{2+}-dependent K^+ channel from transverse tubule membranes isolated from rabbit skeletal muscle. *Proc. Natl. Acad. Sci .USA.* 79:805–809.

Liman, E.R., P. Hess, F. Weaver, and G. Koren. 1991. Voltage-sensing residues in the S4 region of a mammalian K^+ channel. *Nature*

(Lond.). 353:752–756.

Liu, D.T., G.R. Tibbs, and S.A. Siegelbaum. 1996. Subunit stoichiometry of cyclic nucleotide-gated channels and effects of subunit order on channel function. *Neuron*. 16:983–990.

Logothetis, D.E., B.F. Kammen, K. Lindpaintner, D. Bisbas, and G.B. Nadal. 1993. Gating charge differences between two voltage-gated K+ channels are due to the specific charge content of their respective S4 regions. *Neuron*. 10:1121–1129.

Lopez, G.A., Y.N. Jan, and L.Y. Jan. 1991. Hydrophobic substitution mutations in the S4 sequence alter voltage-dependent gating in Shaker K^+ channels. *Neuron*. 7:327–336.

MacKinnon, R. 1991. Determination of the subunit stoichiometry of a voltage-activated potassium channel. *Nature (Lond.)*. 350: 232–235.

MacKinnon, R., R.W. Aldrich, and A.W. Lee. 1993. Functional stoichiometry of Shaker potassium channel inactivation. *Science (Wash. DC)*. 262:757–759.

MacKinnon, R., and C. Miller. 1989. Functional modification of a Ca^{2+}-activated K^+ channel by trimethyloxonium. *Biochemistry*. 28: 8087–8092.

Magleby, K.L., and B.S. Pallotta. 1983. Burst kinetics of single calcium-activated potassium channels in cultured rat muscle. *J. Physiol. (Camb.)*. 344:605–623.

Mannuzzu, L.M., M.M. Moronne, and E.Y. Isacoff. 1996. Direct physical measure of conformational rearrangement underlying potassium channel gating. *Science (Wash. DC)*. 271:213–216.

Marks, T.N., and S.W. Jones. 1992. Calcium currents in the A7r5 smooth muscle-derived cell line. An allosteric model for calcium channel activation and dihydropyridine agonist action. *J. Gen. Physiol.* 99:367–390.

Markwardt, F., and G. Isenberg. 1992. Gating of maxi K+ channels studied by Ca2+ concentration jumps in excised inside-out multi-channel patches (myocytes from guinea pig urinary bladder). *J. Gen. Physiol.* 99:841–862.

Mayer, E.A., D.D. Loo, W.J. Snape, and G. Sachs. 1990. The activation of calcium and calcium-activated potassium channels in mammalian colonic smooth muscle by substance P. *J. Physiol. (Camb.)*. 420:47–71.

McCobb, D.P., N.L. Fowler, T. Featherstone, C.J. Lingle, M. Saito, J.E. Krause, and L. Salkoff. 1995. A human calcium-activated potassium channel gene expressed in vascular smooth muscle. *Am. J. Physiol.* 269:H767–H777.

McManus, O.B. 1991. Calcium-activated potassium channels: regulation by calcium. *J. Bioenerg. Biomembr.* 23:537–560.

McManus, O.B., A.L. Blatz, and K.L. Magleby. 1985. Inverse relationship of the durations of adjacent open and shut intervals for Cl and K channels. *Nature (Lond.)*. 317:625–627.

McManus, O.B., L.M. Helms, L. Pallanck, B. Ganetzky, R. Swanson, and R.J. Leonard. 1995. Functional role of the beta subunit of high conductance calcium-activated potassium channels. *Neuron*. 14:645–650.

McManus, O.B., and K.L. Magleby. 1988. Kinetic states and modes of single large-conductance calcium-activated potassium channels in cultured rat skeletal muscle. *J. Physiol. (Camb.)*. 402:79–120.

McManus, O.B., and K.L. Magleby. 1991. Accounting for the Ca(2+)-dependent kinetics of single large-conductance Ca(2+)-activated K+ channels in rat skeletal muscle. *J. Physiol. (Camb.)*. 443:739–777.

Meera, P., M. Wallner, Z. Jiang, and L. Toro. 1996. A calcium switch for the functional coupling between alpha (hslo) and beta subunits (KV,Ca beta) of maxi K channels. *FEBS Lett.* 382:84–88.

Methfessel, C., and G. Boheim. 1982. The gating of single calcium-dependent potassium channels is described by an activation/blockade mechanism. *Biophys. Struct. Mech.* 9:35–60.

Moczydlowski, E., and R. Latorre. 1983. Gating kinetics of Ca2+-activated K+ channels from rat muscle incorporated into planar lipid bilayers. Evidence for two voltage-dependent $Ca2^+$ binding reactions. *J. Gen. Physiol.* 82:511–542.

Monod, J., J. Wyman, and J.P. Changeux. 1965. On the nature of allosteric transitions: a plausible model. *J. Mol. Biol.* 12:88–118.

Murcott, T.H., H. Gutfreund, and H. Muirhead. 1992. The cooperative binding of fructose-1,6-bisphosphate to yeast pyruvate kinase. *EMBO (Eur. Mol. Biol. Organ.) J.* 11:3811–3814.

Neet, K.E. 1995. Cooperativity in enzyme function: equilibrium and kinetic aspects. *Methods Enzymol.* 249:519–567.

Oberhauser, A., O. Alvarez, and R. Latorre. 1988. Activation by divalent cations of a Ca2+-activated K+ channel from skeletal muscle membrane. *J. Gen. Physiol.* 92:67–86.

Ottolia, M., F. Noceti, R. Olcese, M. Wallner, E. Stefani, and L. Toro. 1996. Charge movement in a voltage and Ca^{2+} sensitive potassium channel (*hslo*). *Biophys. J.* 70:A193.

Pallotta, B.S. 1985. Calcium-activated potassium channels in rat muscle inactivate from a short-duration open state. *J. Physiol. (Camb.)*. 363:501–516.

Papazian, D.M., L.C. Timpe, Y.N. Jan, and L.Y. Jan. 1991. Alteration of voltage-dependence of Shaker potassium channel by mutations in the S4 sequence. *Nature (Lond.)*. 349:305–310.

Pauling, L. 1935. The oxygen equilibrium of hemoglobin and its structural interpretation. *Proc. Natl. Acad. Sci. USA*. 21:186–191.

Perez, G., A. Lagrutta, J.P. Adelman, and L. Toro. 1994. Reconstitution of expressed KCa channels from Xenopus oocytes to lipid bilayers. *Biophys. J.* 66:1022–1027.

Perutz, M. 1989. Mechanisms of cooperativity and allosteric regulation in proteins. Cambridge University Press, New York. pp. 101.

Perutz, M.F. 1976. Haemoglobin: structure, function and synthesis. *Br. Med. Bull.* 32:193–194.

Reinhart, P.H., S. Chung, and I.B. Levitan. 1989. A family of calcium-dependent potassium channels from rat brain. *Neuron*. 2: 1031–1041.

Segal, Y., and L. Reuss. 1990. Maxi K^+ channels and their relationship to the apical membrane conductance in Necturus gallbladder epithelium. *J. Gen. Physiol.* 95:791–818.

Seoh, S., D. Sigg, D.M. Papazian, and F. Bezanilla. 1996. Voltage-sensing residues in the S2 and S4 segments of the *shaker* K^+ channel. *Neuron*. 16:1159–1167.

Shen, K.Z., A. Lagrutta, N.W. Davies, N.B. Standen, J.P. Adelman, and R.A. North. 1994. Tetraethylammonium block of Slowpoke calcium-activated potassium channels expressed in Xenopus oocytes: evidence for tetrameric channel formation. *Pflugers Arch.* 426:440–445.

Sheppard, D.N., F. Giraldez, and F.V. Sepulveda. 1988. Kinetics of voltage- and Ca2+ activation and Ba2+ blockade of a large-conductance K+ channel from Necturus enterocytes. *J. Membr. Biol.* 105:65–75.

Sigworth, F.J. 1994. Voltage gating of ion channels. *Q. Rev. Biophys.* 27:1–40.

Singer, J.J., and J.J. Walsh. 1987. Characterization of calcium-activated potassium channels in single smooth muscle cells using the patch-clamp technique. *Pflugers Arch.* 408:98–111.

Solaro, C.R., C. Nelson, A. Wei, L. Salkoff, and C.J. Lingle. 1995. Cytoplasmic Mg^{2+} modulates Ca^{2+}-dependent activation of mslo by binding to a low affinity site on the channel core. *Biophys. J.* 68:A30.

Stevens, C.F. 1978. Interactions between intrinsic membrane protein and electric field. An approach to studying nerve excitability. *Biophys. J.* 22:295–306.

Tabcharani, J.A., and S. Misler. 1989. $Ca2^+$-activated K+ channel in rat pancreatic islet B cells: permeation, gating and blockade by

cations. *Biochim. Biophys. Acta.* 982:62–72.

Tibbs, G.R., E.H. Goulding, and S.A. Siegelbaum. 1995. Spontaneous opening of cyclic nucleotide-gated channels support an allosteric model of activation. *Biophys. J.* 68:A253.

Toro, L., F. Noceti, M. Ottalia, P. Meera, M. Wallner, R. Latorre, and E. Stefani. 1996. Towards an understanding of how voltage and Ca^{2+} operate in a maxi K channel. *Biophys. J.* 70:A233.

Tseng-Crank, J., C.D. Foster, J.D. Krause, R. Mertz, N. Godinot, T.J. DiChiara, and P.H. Reinhart. 1994. Cloning, expression, and distribution of functionally distinct Ca(2+)-activated K+ channel isoforms from human brain. *Neuron.* 13:1315–1330.

Varnum, M.D., and W.N. Zagotta. 1996. Subunit interactions in the activation of cyclic nucleotide-gated ion channels. *Biophys. J.* 70: 2667–2679.

Wallner, M., P. Meera, M. Ottolia, R. Kaczorowski, R. Latorre, M.L. Garcia, E. Stefani, and L. Toro. 1995. Characterization of and modulation by a β-subunit of a human maxi K_{Ca} channel cloned from myometrium. *Receptors Channels.* 3:185–199.

Wei, A., and L. Salkoff. 1986. Occult Drosophila calcium channels and twinning of calcium and voltage-activated potassium channels. *Science (Wash. DC).* 233:780–782.

Wei, A., C. Solaro, C. Lingle, and L. Salkoff. 1994. Calcium sensitivity of BK-type K_{Ca} channels determined by a separable domain. *Neuron.* 13:671–681.

Wong, B.S., H. Lecar, and M. Adler. 1982. Single calcium-dependent potassium channels in clonal anterior pituitary cells. *Biophys. J.* 39:313–317.

Wu, C.W., and G.G. Hammes. 1973. Relaxation spectra of aspartate transcarbamylase. Interaction of the native enzyme with an adenosine 5′-triphosphate analog. *Biochemistry.* 12:1400–1408.

Wu, Y.C., J.J. Art, M.B. Goodman, and R. Fettiplace. 1995. A kinetic description of the calcium-activated potassium channel and its application to electrical tuning of hair cells. *Prog. Biophys. Mol. Biol.* 63:131–158.

Wyman, J., and S.J. Gill. 1990. Binding and Linkage. University Science Books, Mill Valley, CA. pp. 330.

Yang, N., A.J. George, and R. Horn. 1996. Molecular basis of charge movement in voltage-gated sodium channels. *Neuron.* 16:113–122.

Yang, N., and R. Horn. 1995. Evidence for voltage-dependent S4 movement in sodium channels. *Neuron.* 15:213–218.

Zagotta, W.N., T. Hoshi, and R.W. Aldrich. 1994*a.* Shaker potassium channel gating. III: Evaluation of kinetic models for activation. *J. Gen. Physiol.* 103:321–362.

Zagotta, W.N., T. Hoshi, J. Dittman, and R.W. Aldrich. 1994*b.* Shaker potassium channel gating. II: Transitions in the activation pathway. *J. Gen. Physiol.* 103:279–319.

Zagotta, W.N., and S.A. Siegelbaum. 1996. Structure and function of cyclic nucleotide-gated channels. *Annu. Rev. Neurosci.* 19:235–263.